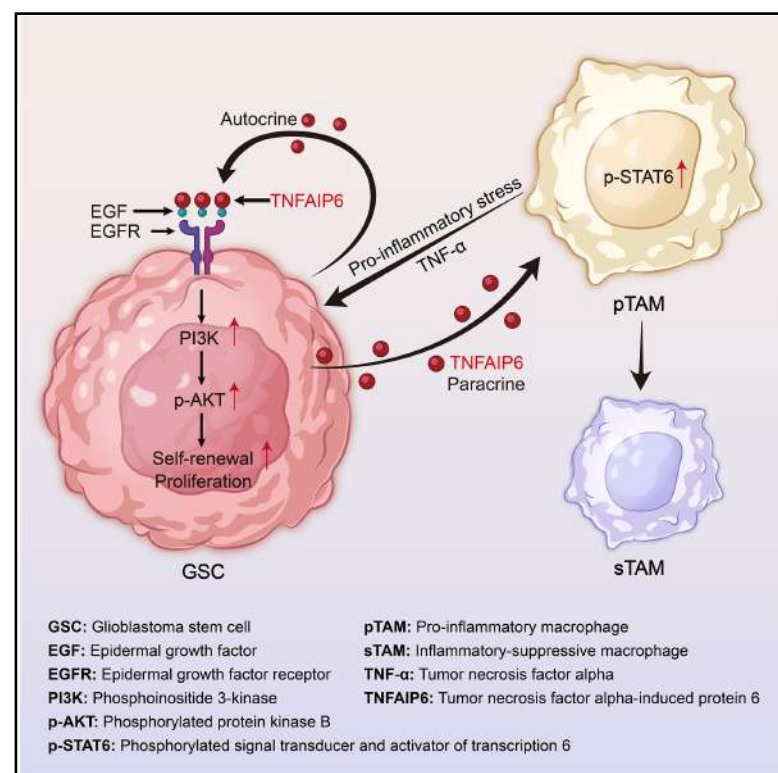


Developmental Cell

Stress-induced pro-inflammatory glioblastoma stem cells secrete TNFAIP6 to enhance tumor growth and induce suppressive macrophages

Graphical abstract



Authors

Danling Gu, Lang Hu, Kailin Yang, ..., Junxia Zhang, Jeremy N. Rich, Xiuxing Wang

Correspondence

liujian623@njucm.edu.cn (J.L.), zhangqian01@njmu.edu.cn (Q.Z.), zjx232@njmu.edu.cn (J.Z.), drjeremyrich@gmail.com (J.N.R.), drxiuxingwang@163.com (X.W.)

In brief

Gu et al. show that pro-inflammatory macrophage (pTAM)-derived pro-inflammatory stress maintains glioblastoma (GBM) stem cell (GSC) proliferation and self-renewal. TNFAIP6, induced by TNF- α , promotes GBM growth through binding EGF and prolonging EGFR-PI3K-AKT signaling in GSCs while converting pTAMs to suppressive TAMs, suggesting that TNFAIP6 is an effective target for GBM therapy.

Highlights

- Pro-inflammatory stress from pTAMs maintains GSC proliferation and self-renewal
- TNFAIP6 binds EGF and prolongs EGFR-PI3K-AKT signaling in GSCs to promote tumor growth
- GSCs secrete TNFAIP6 to transform macrophages from pTAMs to inflammatory-suppressive phenotype
- Pharmacologic targeting of TNFAIP6 by colistin inhibits GBM tumor growth *in vitro* and *in vivo*

Article

Stress-induced pro-inflammatory glioblastoma stem cells secrete TNFAIP6 to enhance tumor growth and induce suppressive macrophages

Danling Gu,^{1,2,3,16} Lang Hu,^{2,3,4,16} Kailin Yang,^{5,16} Wei Yuan,^{6,16} Danyang Shan,^{2,3,16} Jiancheng Gao,^{2,3,16} Jiahuang Li,⁷ Ryan C. Gimple,⁸ Deobrat Dixit,⁹ Zhe Zhu,¹⁰ Daqi Li,^{2,3,9} Qiulian Wu,⁹ Zhumei Shi,⁴ Yingyi Wang,^{3,4} Ningwei Zhao,¹¹ Kun Yang,¹² Junfei Shao,¹ Fan Lin,² Qianghu Wang,³ Guangfu Jin,³ Yun Chen,^{1,3} Xu Qian,³ Zhibin Hu,³ Chaojun Li,³ Nu Zhang,¹³ Yongping You,^{3,4} Jian Liu,^{14,*} Qian Zhang,^{2,3,*} Junxia Zhang,^{3,4,*} Jeremy N. Rich,^{9,*} and Xiuxing Wang^{1,2,3,4,15,17,*}

¹The Affiliated Wuxi People's Hospital of Nanjing Medical University, Wuxi People's Hospital, Wuxi Medical Center, Nanjing Medical University, Wuxi 214000, Jiangsu, China

²National Health Commission Key Laboratory of Antibody Techniques, Department of Cell Biology, Jiangsu Provincial Key Laboratory of Human Functional Genomics, School of Basic Medical Sciences, Nanjing Medical University, Nanjing 211166, Jiangsu, China

³Institute for Brain Tumors, Jiangsu Key Laboratory of Cancer Biomarkers, Prevention and Treatment, Collaborative Innovation Center for Cancer Personalized Medicine, Nanjing Medical University, Nanjing 210029, Jiangsu, China

⁴Department of Neurosurgery, The First Affiliated Hospital of Nanjing Medical University, Nanjing 210029, Jiangsu, China

⁵Department of Radiation Oncology, Taussig Cancer Center, Cleveland Clinic, Cleveland, OH 44195, USA

⁶Department of Pathology, The Yancheng Clinical College of Xuzhou Medical University, The First People's Hospital of Yancheng, Yancheng 224005, Jiangsu, China

⁷School of Biopharmacy, China Pharmaceutical University, Jiangsu 211198, China

⁸Department of Medicine, Washington University School of Medicine, Washington University in St Louis, St. Louis, MO 63110, USA

⁹Department of Neurology, University of Pittsburgh Medical Center Hillman Cancer Center, Pittsburgh, PA 15213, USA

¹⁰Department of Pathology and Cell Biology, Columbia University Irving Medical Center, New York, NY 10032, USA

¹¹China Exposomics Institute, 781 Cai Lun Road, Shanghai 200120, China

¹²Department of Neurosurgery, Zhongda Hospital, Southeast University, Nanjing 210009, Jiangsu, China

¹³Department of Neurosurgery, The First Affiliated Hospital of Sun Yat-Sen University, Guangdong Provincial Key Laboratory of Brain Function and Disease, Guangdong Translational Medicine Innovation Platform, Guangzhou 510080, Guangdong, China

¹⁴School of Pharmacy, Nanjing University of Chinese Medicine, Nanjing 210023, Jiangsu, China

¹⁵Jiangsu Cancer Hospital, Affiliated Cancer Hospital of Nanjing Medical University, Nanjing 210009, Jiangsu, China

¹⁶These authors contributed equally

¹⁷Lead contact

*Correspondence: liujian623@njucm.edu.cn (J.L.), zhangqian01@njmu.edu.cn (Q.Z.), zjx232@njmu.edu.cn (J.Z.), drjeremyrich@gmail.com (J.N.R.), drxiuxingwang@163.com (X.W.)

<https://doi.org/10.1016/j.devcel.2025.04.027>

SUMMARY

Glioblastoma (GBM) is the most aggressive primary intracranial tumor, with glioblastoma stem cells (GSCs) enforcing the intratumoral hierarchy. The inflammatory microenvironment influences tumor development at varying stages, while the underlying mechanism of GSCs facing pro-inflammatory stress remains unclear. Here, we show that, in human GBM, pro-inflammatory stress from pro-inflammatory macrophages (pTAMs) maintains GSC proliferation and self-renewal. Tumor necrosis factor alpha-induced protein 6 (TNFAIP6), as a responder in patient-derived GSCs to pro-inflammatory stress tumor necrosis factor alpha (TNF- α) from human pTAMs, promotes tumor growth through binding epidermal growth factor (EGF) and prolonging EGF receptor (EGFR)-phosphatidylinositol 3-kinase (PI3K)-protein kinase B (AKT) signaling activation. Meanwhile, pro-inflammatory stress-induced patient-derived GSCs secrete TNFAIP6 to transform macrophage phenotype from pTAMs to inflammatory-suppressive macrophages (sTAMs). Collectively, pharmacological or genetic disruption of TNFAIP6 autocrine and paracrine communication between patient-derived GSCs and TAMs inhibited GSC proliferation and self-renewal *in vitro* and in patient-derived xenograft tumor-bearing mice, suggesting that TNFAIP6 is an effective target for GBM therapy.

INTRODUCTION

Glioblastoma (GBM) is the most common and aggressive primary intracranial tumor, with a median survival averaging one

and a half years after initial diagnosis.^{1,2} Glioblastoma stem cells (GSCs), a subpopulation of GBM cells functionally defined by self-renewal and tumor-initiating activity, contribute to driving GBM growth through their capacities of proliferation, invasion,

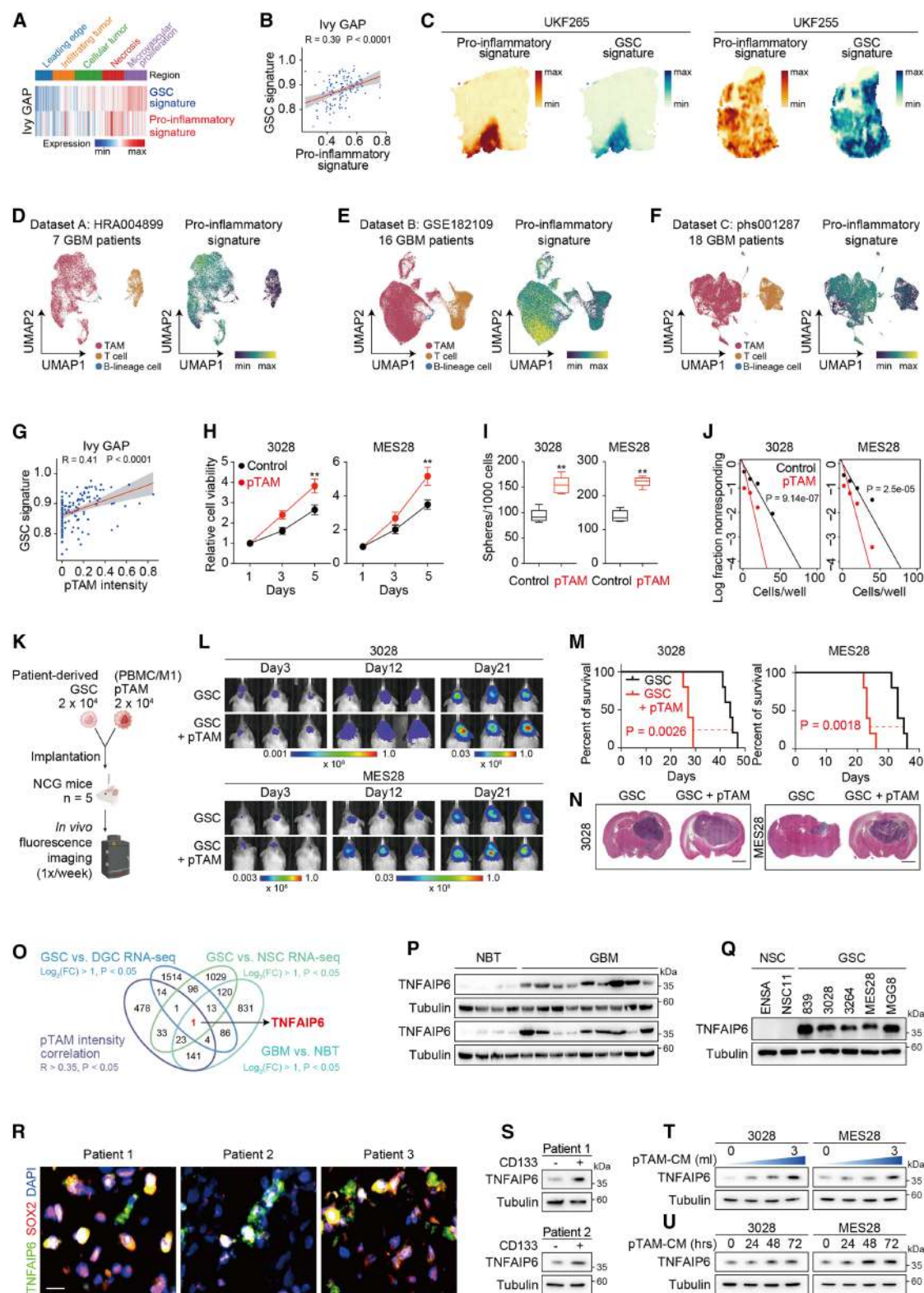


Figure 1. Pro-inflammatory stress induces TNFAIP6 in GSCs

(A) Heatmap showing pro-inflammatory signature associated with GSC signature.
(B) Correlation between pro-inflammatory signature and GSC signature.
(C) Examples of spatial expression patterns of pro-inflammatory and GSC signatures.

(legend continued on next page)

angiogenesis, suppression of anti-tumor immune responses, and chemo-radiotherapy resistance.^{3–6} GSCs actively interact with other cells in the tumor microenvironment (TME) to promote malignant progression in GBM.^{7–11} Given the pivotal role of GSCs in GBM, targeting GSCs and their interactions with other components of the TME has the potential to improve GBM treatment.

Inflammation, irrespective of its occurrence in the context of a tumor-elicited situation or in a therapeutic process, has a great effect on the composition of the TME and particularly on the plasticity of both tumor cells and other cells in the ecosystem.¹² It has become clear now that the immune system can play significant pro- and anti-tumorigenic roles at all stages of tumorigenesis.^{12–14} It is generally believed that pro-inflammatory stress counteracts cancer development and leads to tumor death.^{12,14,15} GSCs live in a niche that consists of astrocytes, microglia, endothelial cells, tumor-associated macrophages (TAMs), and T cells.^{10,12,16,17} However, the characteristics of inflammation in the GBM microenvironment and its relationship with GSCs remain unclear and warrant further exploration.

GSCs actively remodel the TME and, in turn, receive critical maintenance cues from their niches.¹⁸ It is recognized that TAMs can be functionally categorized into pro-inflammatory macrophages (pTAMs) and inflammatory-suppressive macrophages (sTAMs) types. pTAMs exhibit an M1 macrophage-like phenotype, while sTAMs display properties of M2-like macrophages and express M2-specific markers.^{19,20} TAMs are abundant in the GBM microenvironment and are important in supporting malignant growth and progression. At the functional level, sTAMs maintain GSC self-renewal and play immunosuppressive roles in the TME^{9,21}; however, how GSCs respond to the cell-cell communication of pTAMs remains elusive.

Tumor necrosis factor alpha-induced protein 6 (TNFAIP6) has been implicated in regulating anti-inflammatory functions in several diseases, including gastric cancer, brain injury, and lung injury.^{22–24} TNFAIP6 is essential for macrophage phenotype transition in disease models such as acute lung injury.²⁴ Mesen-

chymal stem cells secrete TNFAIP6 to modulate the inflammatory microenvironment by inhibiting the activation of the Toll-like receptor 4 (TLR4)/Myeloid differentiation primary response 88 (MyD88)/nuclear factor κ B (NF- κ B) pathway in spinal microglia.²⁵ High expression of TNFAIP6 indicates a poor prognosis in GBM,²⁶ but its role between GSCs and TAMs in GBM is unexplored.

Using interactive multiomic analyses and functional studies, we identified pro-inflammatory stress from pTAMs that maintain GSC proliferation and self-renewal. TNFAIP6, as a responder in GSCs to pro-inflammatory stress tumor necrosis factor alpha (TNF- α) from pTAMs, promotes GSC-associated tumor growth through binding epidermal growth factor (EGF) and prolonging EGF receptor (EGFR)-phosphoinositide 3-kinase (PI3K)-protein kinase B (AKT) signaling activation. Meanwhile, pro-inflammatory stress-induced GSCs secrete TNFAIP6 to induce phenotype transformation of pTAMs to sTAMs. The pharmacological or genetic disruption of TNFAIP6 autocrine and paracrine communication between GSCs and TAMs inhibited GSC proliferation and self-renewal *in vitro* and *in vivo*, which will advance the therapeutic development against GBM.

RESULTS

Pro-inflammatory stress induces TNFAIP6 in GSCs

To characterize the pro-inflammatory phenotype and its relationship with GSCs, we interrogated the anatomic transcriptional atlas of human GBM, Ivy Glioblastoma Atlas Project (Ivy GAP) dataset,²⁷ and identified that the pro-inflammatory signature demonstrated a significantly positive correlation with the GSC signature in GBM ($R = 0.39$; $p < 0.0001$) (Figures 1A and 1B). Then, we leveraged a reported spatial multiomics analysis of GBM²⁸ and revealed that the pro-inflammatory signature and GSC signature were highly colocalized in patient-derived GBM specimens (Figures 1C and S1A), which encouraged us to further pursue the exact cell types of pro-inflammatory stress in GBM. Using one in-house single-cell

(D–F) UMAP visualization of expression patterns of pro-inflammatory signature in GBM at the single-cell level.

(G) Correlation between pTAM intensity and GSC signature.

(H) Relative cell growth of GSCs co-cultured with PBMC-induced pTAMs or GSCs alone, as measured by CellTiter-Glo assay. Data are presented as the mean \pm SEM of six independent experiments. ** $p < 0.01$.

(I) Quantification of the number of spheres formed by GSCs co-cultured with PBMC-induced pTAMs or GSCs alone. Data are presented as the mean \pm SEM of six independent experiments. ** $p < 0.01$.

(J) The extreme limiting dilution assays (ELDAs) reveal the sphere formation of GSCs co-cultured with PBMC-induced pTAMs or GSCs alone. Data are presented from three independent experiments. ** $p < 0.01$.

(K) Schematic model that illustrates implantation of patient-derived GSCs with or without co-implantation of pTAMs into the brains of immunocompromised mice. Created in BioRender. Wang, X. (2025) <https://BioRender.com/t65t054>.

(L–N) Representative *in vivo* bioluminescent images of NCG immunocompromised mice bearing intracranial xenografts (L). Kaplan-Meier survival curves of NCG immunocompromised mice ($n = 5$ for each group) are shown (M). p values were calculated using the log-rank test. Representative images of H&E-stained coronal sections of tumor-bearing brains are shown (N). Scale bar, 2 mm.

(O) Venn diagram showing the overlap of highly expressed targets.

(P) Immunoblot assessment of TNFAIP6 expression across 18 GBM and 4 NBT. Tubulin was used as a loading control.

(Q) Immunoblot assessment of TNFAIP6 expression across 2 NSC lines and 5 GSC lines. Tubulin was used as a loading control.

(R) Representative images of immunofluorescent staining showing the TNFAIP-positive cells (green) and SOX2-positive cells (red) in three human primary GBM specimens. Scale bar, 10 μ m.

(S) Immunoblot assessment of TNFAIP6 expression in matched CD133-positive and CD133-negative cells from two fresh GBM surgical specimens. Tubulin was used as a loading control.

(T and U) Immunoblot assessment of TNFAIP6 protein levels. GSCs were treated with pTAMs supernatant over a concentration (T) or time course (U). Tubulin was used as a loading control.

See also Figures S1 and S2.

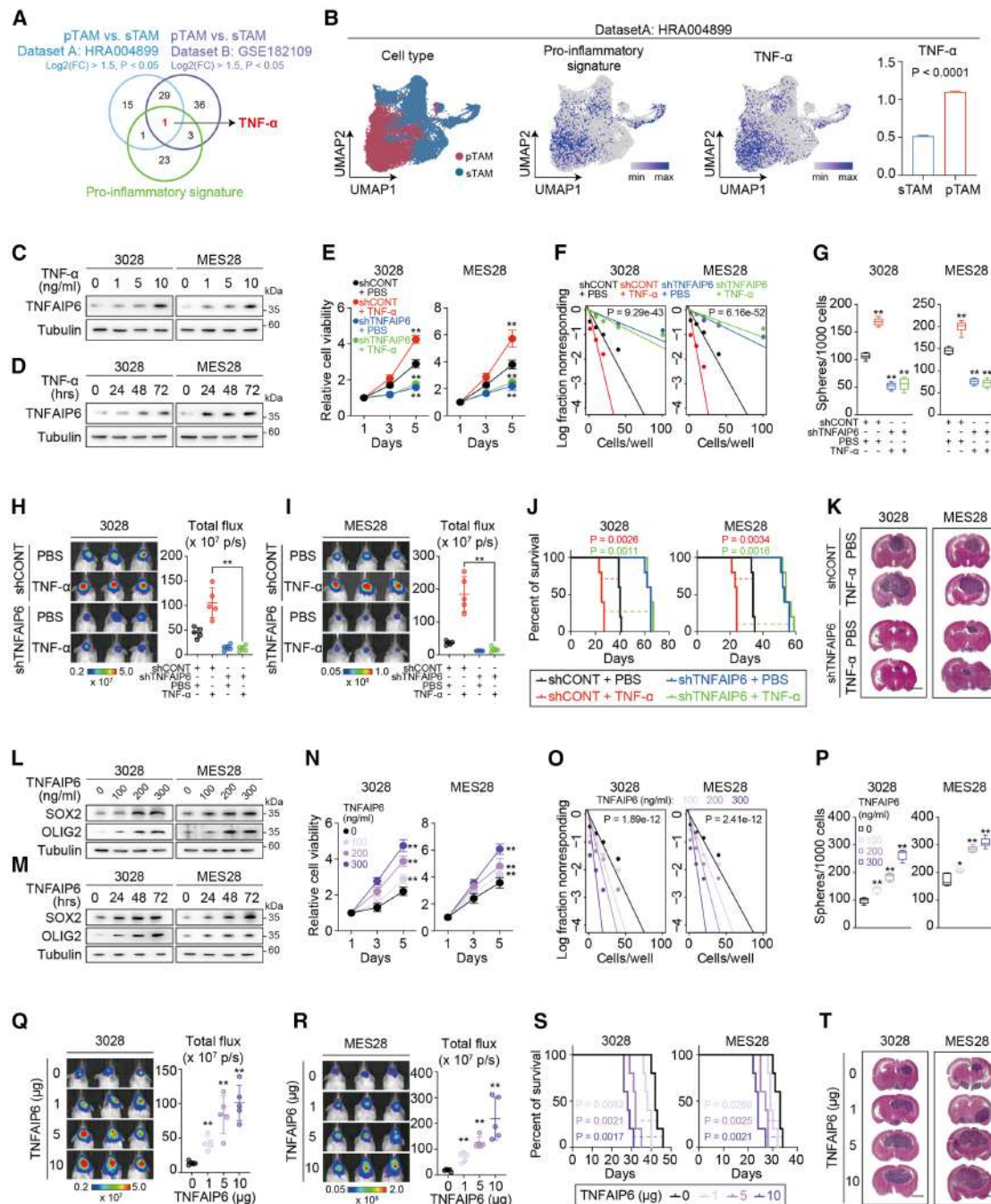


Figure 2. TNFAIP6 maintains GSC self-renewal and tumor growth

(A) Venn diagram showing the overlap of highly expressed targets in pTAMs.

(B) UMAP visualization of pTAM and sTAM in GBM at the single-cell level (left), expression patterns of pro-inflammatory signature and TNF- α (middle), and the relative expression of TNF- α in pTAM and sTAM (right).

(C and D) Immunoblot assessment of TNFAIP6 protein levels. GSCs were treated with TNF- α over a concentration (C) or time (D) course. Tubulin was used as a loading control.

(E) Relative cell growth of GSCs treated with shCONT, TNF- α (10 ng/mL) alone, shTNFAIP6-1 alone, or a combination of shTNFAIP6-1 and TNF- α (10 ng/mL), as measured by CellTiter-Glo assay. Data are presented as the mean \pm SEM of six independent experiments. $^{**}p < 0.01$.

(F) The ELDA reveal the sphere formation of GSCs treated with shCONT, TNF- α (10 ng/mL) alone, shTNFAIP6-1 alone, or a combination of shTNFAIP6-1 and TNF- α (10 ng/mL). Data are presented from three independent experiments. $^{**}p < 0.01$.

(G) Quantification of the number of spheres formed by GSCs treated with shCONT, TNF- α (10 ng/mL) alone, shTNFAIP6-1 alone, or a combination of shTNFAIP6-1 and TNF- α (10 ng/mL). Data are presented as the mean \pm SEM of six independent experiments. $^{**}p < 0.01$.

(legend continued on next page)

RNA sequencing (scRNA-seq) of seven patient-derived GBM samples (dataset A: NGDC: HRA004899), two published datasets of GBM, an scRNA-seq of 16 fresh samples (dataset B: GEO: GSE182109),²⁹ and a single-nuclei RNA sequencing (snRNA-seq) dataset of 18 frozen samples (dataset C: CPTAC: phs001287),³⁰ we profiled the pro-inflammatory signature pattern in GBM-infiltrating immune cells and identified that pTAMs account for the majority of pro-inflammatory immune cells in the GBM microenvironment (Figures 1D–1F). Remarkably, pTAM intensity showed a significant positive correlation with the GSC signature in the Ivy GAP dataset²⁷ (Figure 1G). Based on these findings, we hypothesize that pro-inflammatory stress from pTAMs maintains GSCs in GBM. We then co-cultured the peripheral blood mononuclear cell (PBMC)-induced M1-like macrophages (pTAMs), as previously reported,^{31,32} with patient-derived GSCs to evaluate the function of pTAMs in the tumor niche. pTAMs increased the GSC proliferation, cell viability, and self-renewal (Figures 1H–1J and S1A–S1F). To investigate the *in vivo* function of pTAMs in tumor propagation, we transplanted two patient-derived GSCs with or without pTAMs into the brains of immunocompromised mice (Figure 1K). Mice bearing co-implantation of GSCs and pTAMs demonstrated significantly worse overall survival with increased tumor volume than those with GSCs alone (Figures 1L–1N and S1G–S1I). Using a humanized immune system (HIS) mouse model, we also demonstrated that pTAMs promote GSC-associated tumor growth in human hematopoietic stem cell-NOD CRISPR Prkdc Il2r Gamma (huHSC-NCG) mice, underscoring the biological relevance of pTAM-GSC interaction in a more robust animal model (Figures S1J–S1M). Collectively, these data encouraged us to explore the mechanisms underlying the promotion of GSC proliferation and tumorigenesis by pTAMs.

Given that pTAM-GSC interactions promote tumor growth, we interrogated The Cancer Genome Atlas (TCGA) datasets—GBM vs. normal brain tissues (NBTs),³³ RNA sequencing (RNA-seq) data from GSC and neural stem cell (NSC) populations,³⁴ and GSCs and differentiated tumor cells (DGCs) populations³⁵—the *TNFAIP6* overlapping among these comparisons with positive correlation with pTAM intensity in the Ivy GAP dataset,²⁷ suggesting the potential role of *TNFAIP6* in responding to the pro-inflammatory stress from pTAMs in the GSC niches (Figures 1O and S2A–S2D). Notably, the *TNFAIP6* transcripts produce

TNFAIP6 protein, which plays a vital role in inflammatory diseases and tumors.^{22,23,28} Comparing a cohort of 18 GBM and 4 NBT, *TNFAIP6* mRNA and protein levels were elevated in GBM compared with NBT (Figures 1P, S2E, and S2F). Given the similarities between GSCs and NSCs, we compared mRNA and protein levels of *TNFAIP6* in GSCs and two NSC lines, revealing markedly higher levels in GSCs than in NSCs (Figures 1Q and S2G). The *TNFAIP6* epigenetic profile assayed by histone 3 lysine 27 acetyl (H3K27ac) chromatin immunoprecipitation followed by deep sequencing (ChIP-seq)³⁵ revealed activation of the promoter and enhancer regions surrounding the *TNFAIP6* locus in GSCs (Figure S2H). To achieve a more granular analysis, we extracted the subset of tumor cells and found that the GSC signature was enriched in *TNFAIP6*-high GBM cells (Figures S2I–S2R). Immunofluorescent staining of *TNFAIP6* and SRY-box transcription factor 2 (SOX2) in GBM specimens from human patients revealed that *TNFAIP6* was enriched in GBM patients with overlap between *TNFAIP6*- and SOX2-positive tumor cells (Figure 1R). As further confirmation to avoid bias induced by tissue culture or xenografting, we derived matched populations of CD133⁺ and CD133[−] tumor cells from two fresh surgical GBM specimens. The protein levels of *TNFAIP6* were upregulated in CD133⁺ tumor cells relative to CD133[−] tumor cells (Figure 1S). *TNFAIP6* and CD133 were also quantified by immunohistochemistry (IHC) in GBM tumor specimens, which revealed a positive correlation between these two proteins (Figures S2S and S2T). Additionally, *TNFAIP6* was upregulated in GSCs when co-cultured with pTAMs (Figures 1T, 1U, and S2U). Additionally, we demonstrated that conditioned medium (CM) from pTAMs also induced *TNFAIP6* in NSCs, while CM from pTAMs decreased the proliferation of NSCs (Figures S2V–S2X). Taken together, these results support the specific expression of *TNFAIP6* in GSCs, suggesting that it could contribute to GSCs responding to the pTAM-derived pro-inflammatory stress.

TNFAIP6 maintains GSC self-renewal and tumor growth

To understand the contribution of pTAMs in the crosstalk with GSCs, we analyzed the differentially expressed genes in pTAMs vs. sTAMs in two scRNA-seq datasets (dataset A: NGDC: HRA004899; dataset B: GEO: GSE182109) and found the *TNF-α* gene to be dominant (Figures 2A, 2B, and S3A). As a

(H–K) Representative *in vivo* bioluminescence images (left) and quantification (right, $n = 5$ mice per group) of mice bearing the indicated xenografts. Images were acquired when the first neurological sign occurred in any cohort (H and I). Kaplan-Meier survival curves of NCG immunocompromised mice ($n = 5$ for each group) are shown in (J). p values were calculated using the log-rank test. Representative images of H&E-stained coronal sections of tumor-bearing brains are shown in (K). Scale bar, 2 mm.

(L and M) Immunoblot assessment of stemness markers SOX2 and oligodendrocyte transcription factor 2 (OLIG2) protein levels. GSCs were treated with *TNFAIP6* over a concentration (L) or time (M) course. Tubulin was used as a loading control.

(N) Relative cell growth of GSCs treated with *TNFAIP6* over a concentration course, as measured by CellTiter-Glo assay. Data are presented as the mean \pm SEM of six independent experiments. ** $p < 0.01$.

(O) The ELDA reveal the sphere formation of GSCs treated with *TNFAIP6* over a concentration course. Data are presented from three independent experiments. ** $p < 0.01$.

(P) Quantification of the number of spheres formed by GSCs treated with *TNFAIP6* over a concentration course. Data are presented as the mean \pm SEM of six independent experiments. ** $p < 0.01$.

(Q–T) Representative *in vivo* bioluminescence images (left) and quantification (right, $n = 5$ mice per group) of mice bearing the indicated xenografts. Images were acquired when the first neurological sign occurred in any cohort (Q and R). Kaplan-Meier survival curves of NCG immunocompromised mice ($n = 5$ for each group) are shown in (S). p values were calculated using the log-rank test. Representative images of H&E-stained coronal sections of tumor-bearing brains are shown in (T). Scale bar, 2 mm.

See also Figure S3.

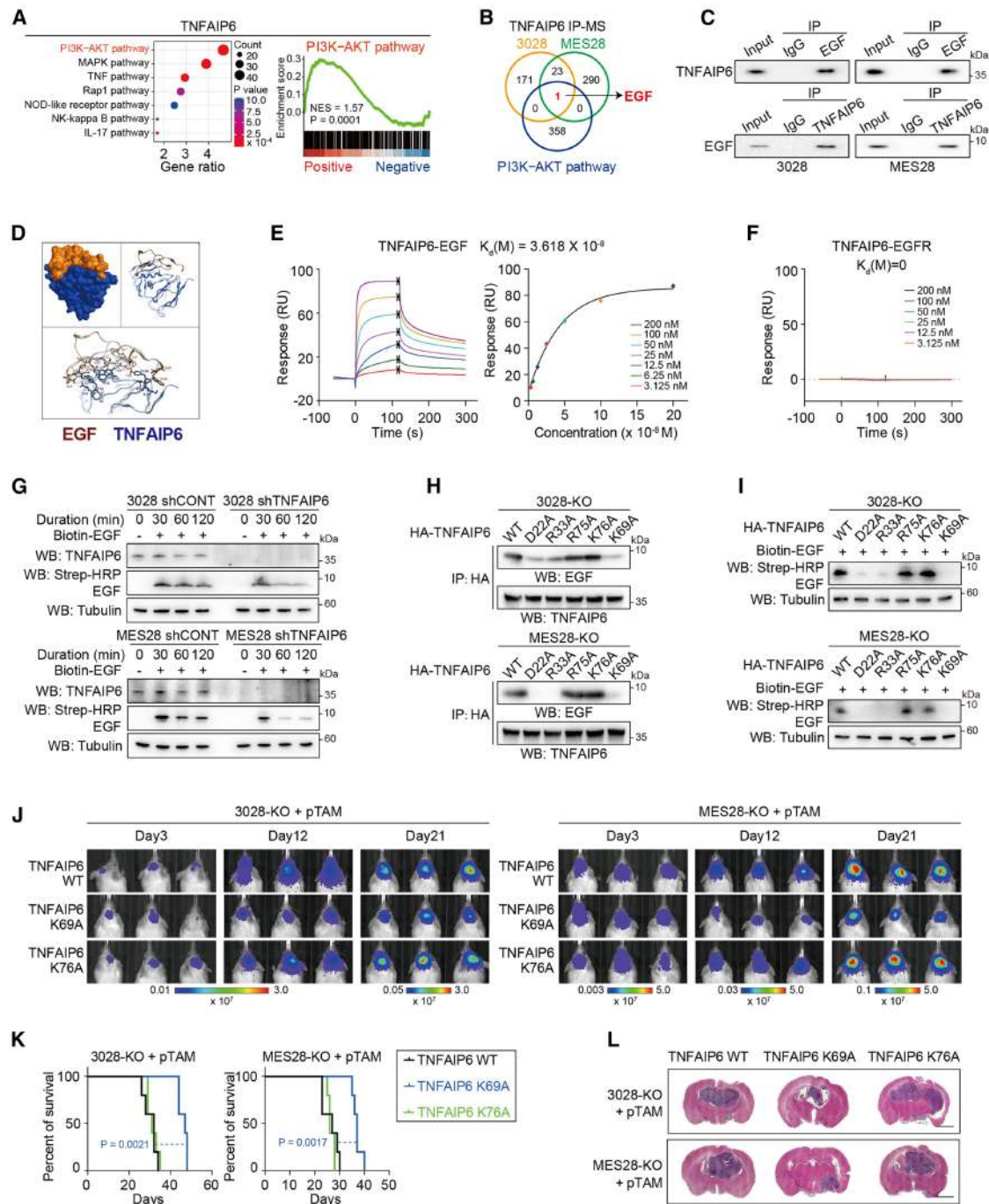


Figure 3. TNFAIP6 directly binds to EGF in GSCs

(A) KEGG enrichment and GSEA of signaling pathways related to TNFAIP6 expression in the TCGA GBM dataset.
 (B) Venn diagram showing the overlap of TNFAIP6-binding proteins in 3028 and MES28 GSCs and PI3K-AKT pathway gene set from KEGG.
 (C) Immunoblot of IP with anti-EGF antibody (upper) or anti-TNFAIP6 antibody (lower) in GSCs, with nonspecific IgG as negative controls.
 (D) Molecular docking analysis of TNFAIP6 with EGF.
 (E) Surface plasmon resonance (SPR) analysis of the interaction between EGF and TNFAIP6.
 (F) SPR analysis of the interaction between EGFR and TNFAIP6.
 (G) Immunoblot assessment of the kinetics of intracellular level of EGF in GSCs transduced with shCONT or shTNFAIP6-1. Tubulin was used as a loading control.
 (H) Immunoblot of IP with anti-HA antibody in TNFAIP6 knockout through transduction with sgTNFAIP6-1 and overexpressing wild-type TNFAIP6 or mutant TNFAIP6 of D22A, R33A, K69A, R75A, and K76A.
 (I) Immunoblot assessment of the EGF levels in 3028-KO and MES28-KO GSCs transduced with overexpressing wild-type TNFAIP6 or mutant TNFAIP6 of D22A, R33A, K69A, R75A, and K76A. Tubulin was used as a loading control.

(legend continued on next page)

pro-inflammatory cytokine, TNF- α has various effects in the response to injury and infection, tumorigenesis, and other physiological processes.^{36–38} We evaluated the function of TNF- α and identified that TNF- α increased GSC proliferation, cell viability, self-renewal, and tumor propagation (Figures S3B–S3J). Meanwhile, to assess the TNFAIP6 expression under the pro-inflammatory stress from TNF- α , we treated patient-derived GSCs with TNF- α over a concentration and a time course. We confirmed the upregulated expression of TNFAIP6 in GSCs, as well as the upregulation of stemness markers, SOX2 and CD133, and the decreased expression of differentiation marker, GFAP (Figures 2C, 2D, S3K, and S3L).

To determine whether TNFAIP6 induced by TNF- α contributes to GSC maintenance, we developed one nontargeting control short hairpin RNA (shRNA), defined as shCONT, and shRNA to knock down *TNFAIP6* expression, designated shTNFAIP6. We treated GSCs expressing shRNA targeting *TNFAIP6* with TNF- α . Knockdown of *TNFAIP6* attenuated the pro-proliferative and stemness maintenance effects of TNF- α (Figures 2E–2G and S3M). We next examined the function of TNF- α -induced TNFAIP6 using an *in vivo* tumorigenesis assay. Immunocompromised mice bearing GSCs treated with TNF- α demonstrated worse overall survival compared with control GSCs, but the *in vivo* effect of TNF- α via intracranial injection was lost when *TNFAIP6* expression was knocked down using shRNA (Figures 2H–2K), suggesting the vital role of TNFAIP6 induced by pTAM-derived TNF- α in GBM. Further, we treated patient-derived GSCs with recombinant TNFAIP6 (rTNFAIP6) over a concentration or time course. Consistently, the stemness markers were upregulated in GSCs (Figures 2L and 2M). Treatment with rTNFAIP6 maintained GSC proliferation, cell viability, self-renewal, and tumor growth (Figures 2N–2T). Collectively, these results strengthened the point that TNFAIP6 is critical for GSC maintenance and tumor growth.

TNFAIP6 directly binds to EGF in GSCs

To understand the molecular mechanisms underlying TNFAIP6-mediated GSC proliferation, we interrogated the TCGA dataset using the Kyoto Encyclopedia of Genes and Genomes (KEGG) and gene set enrichment analysis (GSEA) analysis. We found that PI3K-AKT signaling was positively correlated with TNFAIP6 in GBM (Figure 3A). To identify possible interaction partners mediating the autocrine signaling functions of TNFAIP6 in GSCs, we performed immunoprecipitation (IP) with the anti-TNFAIP6 monoclonal antibody on whole cell lysates from GSCs. The precipitated proteins were analyzed using mass spectrometry (MS). The TNFAIP6 antibody IP preferentially enriched EGF as a top-ranked protein compared with the nonspecific human immunoglobulin G (IgG) negative control (Figures 3B and S4A). Given its role as a surface receptor tyrosine kinase (RTK) ligand and essential function in GSCs, we focused on EGF for further analysis. Reciprocal IP with either an anti-TNFAIP6 antibody or an anti-EGF antibody confirmed that TNFAIP6 interacted with EGF in GSCs (Figure 3C). We

used the ClusPro server³⁹ to perform molecular docking simulations of TNFAIP6 to the EGF domain. The Ramachandran plot indicated that the three-dimensional (3D) structure of the model was consistent (Figure 3D). Next, we performed the surface plasmon resonance (SPR) assay using purified proteins of TNFAIP6 and EGF to evaluate their direct interaction. rTNFAIP6 is effectively bound to immobilized EGF, with a dissociation constant (K_d) of 36.18 nM (Figure 3E). EGFR signaling is critical to tumorigenesis in GBM, but clinical strategies targeting EGFR have not translated into improved patient outcomes, suggesting that understanding the complexity of EGFR signaling may inform therapeutic strategies. These observations prompted us to investigate further whether TNFAIP6 could bind to EGFR and activate PI3K-AKT signaling in GSCs. Intriguingly, TNFAIP6 was not able to bind to EGFR (Figure 3F).

We then sought to determine the functions of TNFAIP6-EGF binding in GSC. We treated GSCs expressing shRNA targeting *TNFAIP6* with biotin-EGF and identified that knockdown of *TNFAIP6* attenuated the EGF levels in GSCs (Figure 3G). We performed the co-staining immunofluorescence and demonstrated that TNFAIP6-associated phospho-EGFR stayed on the cell membrane for 60 min after stimulation, which suggests that TNFAIP6 retains EGF-EGFR signaling on the cell surface for a prolonged period (Figure S4B). To determine the importance of the key residue on TNFAIP6 directly involved in the interaction with EGF, mutant forms of TNFAIP6 were generated through alanine scanning. Residues of the TNFAIP6 protein—specifically D22, R33, R75, K76, and K69—were recognized as potential key sites of the interaction between TNFAIP6 and EGF. Point mutations at residue sites of D22, R33, or K69 of TNFAIP6 decreased its binding affinity with EGF but not at R75 or K76 in IP experiments (Figure 3H). Consistently, mutations at D22, R33, or K69 attenuated the EGF levels in GSCs (Figure 3I). At the cellular level, TNFAIP6 K76A maintained the GSC proliferation and self-renewal, while TNFAIP6 K69A failed to stimulate cellular growth and proliferation or to sustain the expression of stemness markers (Figures S4C–S4G). To investigate the *in vivo* function of tumor propagation, we co-transplanted pTAMs with patient-derived GSCs transduced with wild-type TNFAIP6, TNFAIP6 K69A, or TNFAIP6 K76A into the brains of immunocompromised mice. Mice bearing GSCs harboring TNFAIP6 K69A demonstrated longer overall survival with smaller intracranial tumor volumes compared with mice with GSCs transduced with wild-type TNFAIP6 or TNFAIP6 K76A (Figures 3J–3L). Taken together, these findings indicate that TNFAIP6 acts through direct binding to the EGF and maintains GSCs.

TNFAIP6 prolongs EGFR-PI3K-AKT signaling activation through EGF binding in GSCs

Based on the direct binding of TNFAIP6 to the EGF but not EGFR and the positive correlation between TNFAIP6 and PI3K-AKT signaling, we next asked how TNFAIP6 affects the activation of downstream signaling in GSCs. We treated two patient-derived GSCs (3028 and MES28) with TNFAIP6 protein (300 ng/mL),

(J–L) Representative *in vivo* bioluminescent images of NCG immunocompromised mice bearing intracranial xenografts (J). Kaplan-Meier survival curves of NCG immunocompromised mice ($n = 5$ for each group) are shown in (K). p values were calculated using the log-rank test. Representative images of H&E-stained coronal sections of tumor-bearing brains are shown in (L). Scale bar, 2 mm. See also Figure S4.

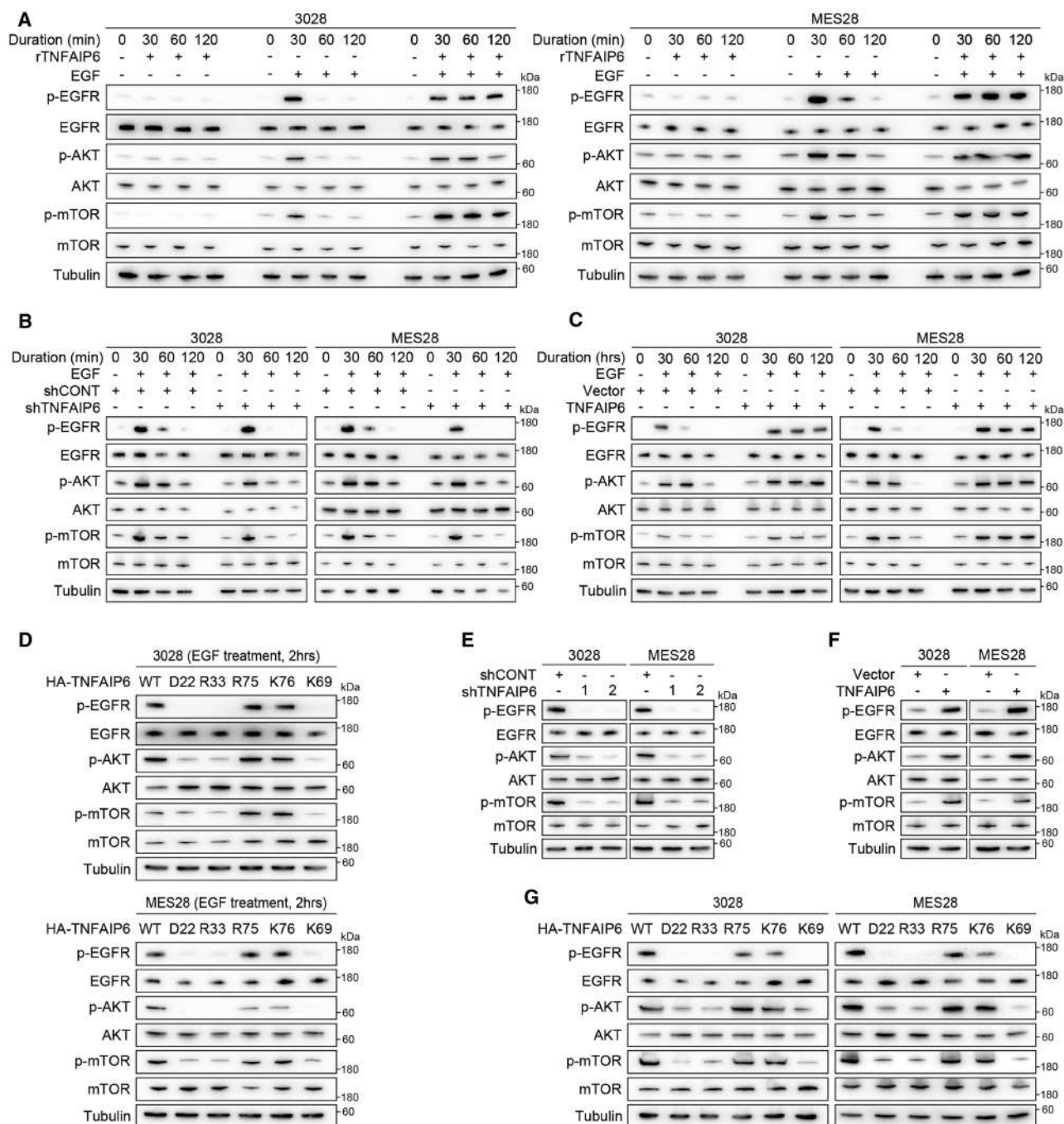


Figure 4. TNFAIP6 prolongs EGFR-PI3K-AKT signaling activation through EGF binding in GSCs

(A) Immunoblot assessment of activated EGFR (p-EGFR), activated AKT (p-AKT), and activated mTOR (p-mTOR) protein levels. 3028 and MES28 GSCs were treated with recombinant TNFAIP6 (rTNFAIP6, 200 ng/mL) alone, EGF (20 ng/mL) alone, or combined rTNFAIP6 and EGF over a time course, in the absence of other growth factors. Tubulin was used as a loading control.

(B) Immunoblot assessment of activated EGFR (p-EGFR), activated AKT (p-AKT), and activated mTOR (p-mTOR) protein levels. GSCs were transduced with shCONT or shTNFAIP6-1 and treated with EGF (20 ng/mL) over a time course without other growth factors. Tubulin was used as a loading control.

(C) Immunoblot assessment of activated EGFR (p-EGFR), activated AKT (p-AKT), and activated mTOR (p-mTOR) protein levels. GSCs were transduced with an empty vector or TNFAIP6 overexpression vector and treated with EGF (20 ng/mL) over a time course without other growth factors. Tubulin was used as a loading control.

(D) Immunoblot assessment of activated EGFR (p-EGFR), activated AKT (p-AKT), and activated mTOR (p-mTOR) protein levels. GSCs were transduced with overexpressing wild-type TNFAIP6 or mutant TNFAIP6 of D22A, R33A, K69A, R75A, and K76A. EGF (20 ng/mL) was treated for 2 h without other growth factors. Tubulin was used as a loading control.

(legend continued on next page)

EGF (20 ng/mL), or both in the absence of other growth factors over a time course. TNFAIP6 alone was not able to induce p-EGFR, p-AKT, and p-mechanistic target of rapamycin kinase (mTOR) in GSCs. By contrast, combined treatment of TNFAIP6 and EGF induced a prolonged activation of EGFR-PI3K-AKT signaling compared with EGF treatment alone (Figure 4A). In loss-of-function studies, knockdown of TNFAIP6 attenuated the activation of EGFR-PI3K-AKT signaling in GSCs on immunoblot (Figure 4B). Reciprocal gain-of-function treatment with TNFAIP6 protein in the absence of other growth factors prolonged the phosphorylation of EGFR, AKT, and mTOR in GSCs (Figure 4C). To examine the significance of TNFAIP6-EGF binding in EGFR-PI3K-AKT signaling activation, we treated two patient-derived GSCs transduced with wild-type TNFAIP6 or mutant TNFAIP6 at D22, R33, R75, K76, and K69 residues with EGF (20 ng/mL) for 2 h in the absence of other growth factors. The activation of phosphorylated EGFR, AKT, and mTOR was maintained in wild-type TNFAIP6, TNFAIP6 R75A, and TNFAIP6 K76A but not TNFAIP6 D22A, TNFAIP6 R33A, or TNFAIP6 K69A GSCs (Figure 4D), suggesting the vital role of TNFAIP6-EGF binding for maintaining EGFR-PI3K-AKT signaling in GSCs. To further clarify the TNFAIP6 impact on EGFR-PI3K-AKT signaling maintenance, we assessed the phosphorylation levels of EGFR, AKT, and mTOR in GSCs expressing shRNA targeting *TNFAIP6* maintained in the complete neural basal medium (NBM). Knockdown of *TNFAIP6* attenuated the EGFR-AKT-mTOR activation (Figure 4E). Conversely, overexpression of *TNFAIP6* induced EGFR-PI3K-AKT signaling in GSCs maintained in the completed NBM (Figure 4F). GSCs transduced with wild-type TNFAIP6, TNFAIP6 R75A, or TNFAIP6 K76A maintained EGFR-PI3K-AKT signaling activation, supporting the role of TNFAIP6-EGF binding in mediating EGFR-PI3K-AKT signaling activation (Figure 4G).

Targeting TNFAIP6-EGF binding suppresses the GSC-associated tumor growth

Our data showed that TNFAIP6, as a responder in GSCs to pro-inflammatory stress TNF- α , promotes GSC-associated tumor growth through binding EGF and prolonging EGFR-PI3K-AKT signaling activation, suggesting TNFAIP6 as a meaningful target for GBM. As inhibitors targeting TNFAIP6 are unavailable, we then developed a pipeline to perform virtual molecular screening with Food and Drug Administration (FDA)-approved drugs according to the TNFAIP6 residues binding EGF (D22, R33, and K69) and focused on colistin, an FDA-approved polymyxin antibiotic (Figure 5A).⁴⁰ Using bio-layer interferometry (BLI), we validated the binding of colistin with TNFAIP6 (Figure 5B). Cell viability assay showed that colistin attenuated GSC proliferation at micromolar concentrations, showing the half maximal inhibitory concentration (IC₅₀) at 14.08 to 50.70 μ M (Figure 5C). We treated patient-derived GSCs with colistin at the concentration

of 20 μ M and found that colistin decreased GSC self-renewal (Figures 5D, 5E, and S4H). IP with the anti-TNFAIP6 or anti-EGF antibody showed that TNFAIP6 failed to bind with EGF when treated with colistin (Figure 5F). With colistin treatment, the activation of EGFR-PI3K-AKT signaling and stemness in GSCs was attenuated (Figures S4I–S4K). Further, colistin inhibited GSC proliferation and self-renewal effectively in GSCs transduced with wild-type TNFAIP6 or TNFAIP6 K76A but failed in GSCs transduced with TNFAIP6 K69A (Figures 5G–5I). Treatment with colistin as a single agent administered intracranially (Figure 5J) extended the survival of mice bearing GSCs with co-transplantation of pTAMs (Figures 5K and 5L). Histologic evaluation of the brains of tumor-bearing mice confirmed that tumor volumes reflected the differences in survival (Figure 5M). These data demonstrated that TNFAIP6 is a promising therapeutic target in GBM.

TNFAIP6 promotes macrophage phenotype switch from pTAMs to sTAMs

Based on prior connections between TNFAIP6 and immune responses, specifically macrophages,^{24,41} we hypothesized that TNFAIP6 acts as a secreted factor to modulate the phenotypes of TAMs in GBM. CM, used for TAMs co-culture, was generated from either control GSCs or GSCs expressing shRNA targeting *TNFAIP6* in growth factor-free conditions. Flow cytometry results showed that CM from two patient-derived GSCs (3028 and MES28) expressing shRNA targeting *TNFAIP6* polarized PBMC-induced TAMs toward a pro-inflammatory phenotype by decreasing the percentage of CD206-positive cells. At the same time, this effect was switched when supplied with TNFAIP6 protein (Figures 6A and 6B). PBMC-induced TAMs co-cultured with CM of GSCs expressing shRNA targeting *TNFAIP6* displayed increased secretion of TNF- α and reduced when supplied with TNFAIP6 protein (Figure 6C), implying that TNFAIP6 maintains sTAMs phenotypes. Signal transducer and activator of transcription 6 (STAT6) is a key signaling pathway in macrophage function, and phosphorylation of STAT6 is a recognized marker of M2-like macrophages (sTAMs).⁴² Tumor-derived primary TAMs, PBMC-induced and Tohoku Hospital Pediatrics-1 (THP-1)-induced pTAMs (M1-like macrophages) were used to further confirm the function of TNFAIP6 on TAMs in the GSC niche. Loss of TNFAIP6 reduced mRNA levels of M2-like markers (Figures S5A–S5C) and attenuated the activation of STAT6 (Figures 6D–6F) in tumor-derived primary TAMs, PBMC-induced TAMs, and THP-1-induced TAMs. Additionally, the loss of TNFAIP6 increased mRNA levels of M1-like markers (Figures S5D and S5E) in PBMC-induced TAMs and THP-1-induced TAMs. We interrogated the in-house scRNA-seq of 7 patient-derived GBM samples (dataset A: NGDC: HRA004899) and a published dataset of GBM, which is an scRNA-seq of 16 fresh samples (dataset B: GEO: GSE182109).²⁹ We then demonstrated that TLR4 is mainly

(E) Immunoblot assessment of activated EGFR (p-EGFR), activated AKT (p-AKT), and activated mTOR (p-mTOR) protein levels. GSCs were transduced with shCONT, shTNFAIP6-1, or shTNFAIP6-2. GSCs were maintained in the completed neural basal medium (NBM). Tubulin was used as a loading control.
(F) Immunoblot assessment of activated EGFR (p-EGFR), activated AKT (p-AKT), and activated mTOR (p-mTOR) protein levels. GSCs were transduced with empty vector or TNFAIP6 overexpression vector. GSCs were maintained in the completed NBM. Tubulin was used as a loading control.
(G) Immunoblot assessment of activated EGFR (p-EGFR), activated AKT (p-AKT), and activated mTOR (p-mTOR) protein levels. GSCs were transduced with overexpressing wild-type TNFAIP6 or mutant TNFAIP6 of D22A, R33A, K69A, R75A, and K76A. GSCs were maintained in the completed NBM. Tubulin was used as a loading control.

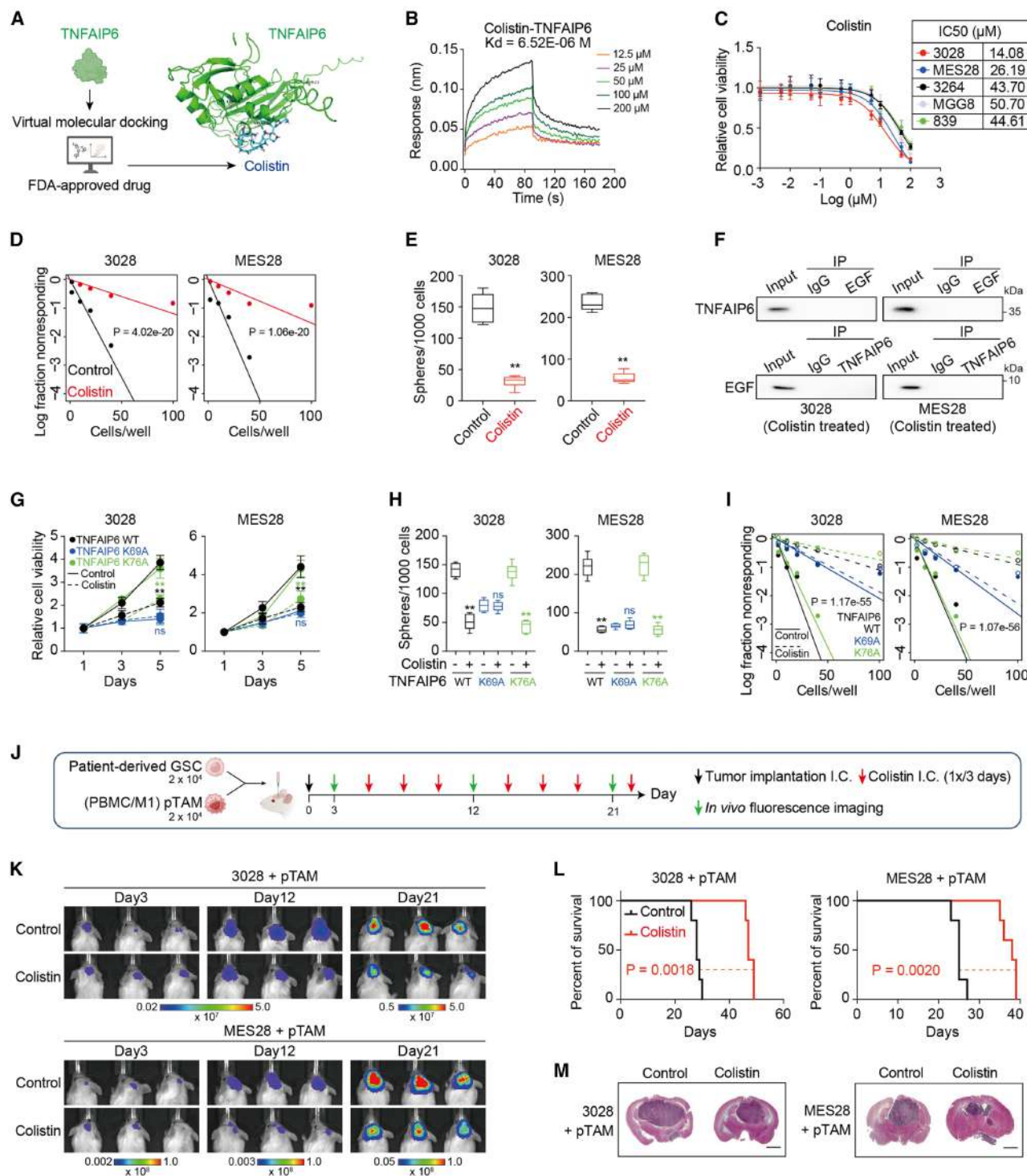


Figure 5. Targeting TNFAIP6-EGF binding suppresses the GSC-associated tumor growth

(A) Workflow of experimental strategy for finding TNFAIP6-targeting drugs (left). Molecular docking analysis of TNFAIP6 with colistin (right).

(B) Bio-layer interferometry (BLI) was used to detect the equilibrium dissociation constant (K_d) between colistin and TNFAIP6.

(C) Dose-response curves for colistin in five patient-derived GSC models.

(D) The ELDAs reveal the sphere formation of GSCs treated with colistin (20 μ M). Data are presented from three independent experiments. ** $p < 0.01$.

(E) Quantification of the number of spheres formed by GSCs treated with colistin (20 μ M). Data are presented as the mean \pm SEM of six independent experiments. ** $p < 0.01$.

(legend continued on next page)

expressed on macrophages in GBM (Figures S5F and S5G). To validate whether this mechanism works in the pTAM-GSC interaction in GBM, we treated pTAMs with rTNFAIP6. IP with an anti-TLR4 antibody confirmed that rTNFAIP6 attenuated the interaction between TLR4 and MYD88 in pTAMs and impaired the downstream NF- κ B signaling, supporting the vital role of TNFAIP6 in switching macrophage phenotype in the GSC niche (Figure S5H). Concordantly, xenografts derived from GSCs transduced with shTNFAIP6 showed a markedly reduced frequency of M2-like macrophages, as measured by CD163 and pan-macrophage marker Iba-1, compared with xenografts derived from GSCs transduced with shCONT (Figures 6G and 6H). These results revealed that TNFAIP6 switches macrophage phenotype from pTAMs to sTAM in GBM.

Given the paracrine function of TNFAIP6 in the GSCs microenvironment, we hypothesized that inhibiting the TAMs phenotype switch combined with colistin may synergize the anti-tumor efficacy. AS1517499 is a pharmacologic inhibitor of STAT6.⁴² To validate the efficacy of this combined therapy *in vivo*, GSCs and pTAMs were implanted into the frontal lobes of immunocompromised mice. Tumor-bearing mice underwent treatment with vehicle control, colistin, AS1517499, or the combination of colistin and AS1517499 (Figure 6I). Intracranial administration of colistin prolonged survival moderately, but survival increased markedly in the group receiving the combination of colistin and AS1517499 (Figures 6J–6L). Taken together, TNFAIP6, the responder in GSCs, altered the main source of pro-inflammatory stress pTAMs to sTAMs, showing an adaptive ability to TME danger. Combined targeting of TNFAIP6 and sTAMs exhibited synergized anti-tumor efficacy.

Pharmacologic targeting of TNFAIP6 augments the anti-tumor efficacy of EGFR inhibition in GBM

Treatment options for recurrent GBM remain ineffective and largely palliative. RTKs, including EGFR, are commonly dysregulated oncogenic pathways in GBM, yet therapies targeting these pathways have repeatedly failed in clinical trials. TNFAIP6-EGF binding prolonged EGFR-PI3K-AKT signaling activation, which suggested combinatorial targeting approaches for improved outcomes. Treatment of GSCs with the EGFR inhibitors osimertinib or gefitinib inhibited GSC proliferation at submicromolar concentrations *in vitro* (Figure 7A). Colistin augmented the efficacy of EGFR inhibitor osimertinib against GSCs (Figure 7B). To further determine the possibility of combinatorial benefit *in vivo*, we implanted pTAMs and GSCs transduced with luciferase

into the brains of immunocompromised mice to interrogate the effect of targeting TNFAIP6 and EGFR on tumor growth. Tumor-bearing mice underwent treatment with vehicle control, colistin, osimertinib, or the combination of colistin and osimertinib (Figure 7C). Combined targeting of TNFAIP6 and EGFR enhanced overall survival and reduced the tumor volume and EGFR activation compared with each monotherapy individually or the vehicle control group in intracranial xenograft models (Figures 7D–7F and S6A). Collectively, our data demonstrated that pharmacologic targeting of TNFAIP6 augments the anti-tumor efficacy of EGFR in GBM.

To generalize our findings of TNFAIP6 dependence to the clinical, we analyzed the TCGA³³ and several GBM datasets.⁴³ We revealed that TNFAIP6 informed poor prognosis in GBM patients (Figures 7G and S6B). Integrating combined TNFAIP6 and EGFR expression levels informed a much poorer prognosis (Figure 7H). To confirm the connection between TNFAIP6 and EGFR in the absence of cell culture, we interrogated the spatial transcriptomics from GBM patient specimens.²⁸ TNFAIP6 levels spatially correlate with EGFR in the GBM spatial transcriptomic dataset (Figure 7I), although not exclusively.

Notably, TNF- α showed no prognostic significance in GBM patients. At the same time, in the TNF- α high group, TNFAIP6 informed poor prognosis, which strengthened our finding that GSCs express TNFAIP6 in response to pro-inflammatory stress TNF- α to promote GSC-associated tumor growth (Figure S6C). Additionally, in agreement with our findings, integrating TNFAIP6 and EGF, or STAT6 expression levels, collectively informed prognosis to a greater degree (Figures S6D and S6E).

To assess the expression of TNFAIP6 in human cancer, we examined bulk RNA-seq datasets through the TCGA with both tumor and normal tissue across 28 tumor types. The expression of TNFAIP6 in tumor vs. normal tissue was highly variable across different tumor types. Ranked by the TNFAIP6 expression in tumors, kidney renal clear cell carcinoma (KIRC), kidney renal papillary cell carcinoma (KIRP), GBM, breast cancer (BRCA), pancreatic adenocarcinoma (PAAD), head and neck squamous cell carcinoma (HNSC), esophageal carcinoma (ESCA), stomach adenocarcinoma (STAD), and ovarian cancer (OV) presented higher TNFAIP6 expression than those in relative normal tissue. In comparison, thymoma (THYM) presented lower TNFAIP6 expression than that in relative normal tissue (Figure S6F). We then interrogated the overall survival in TCGA datasets across those nine tumor types with significant expression differences. TNFAIP6 expression portended a

(F) Immunoblot of IP with anti-EGF antibody (upper) or anti-TNFAIP6 antibody (lower) in GSCs treated with colistin (20 μ M, 48 h), with nonspecific IgG as negative controls.

(G) Relative cell growth of GSCs treated with colistin (20 μ M), as measured by CellTiter-Glo assay. 3028-KO or MES28-KO GSCs were transduced with overexpressing wild-type TNFAIP6 or mutant TNFAIP6 of K69A and K76A. Data are presented as the mean \pm SEM of six independent experiments. ** p < 0.01.

(H) Quantification of the number of spheres formed by GSCs treated with colistin (20 μ M). 3028-KO or MES28-KO GSCs were transduced with overexpressing wild-type TNFAIP6 or mutant TNFAIP6 of K69A and K76A. Data are presented as the mean \pm SEM of six independent experiments. ** p < 0.01.

(I) The ELDA reveal the sphere formation of GSCs treated with colistin (20 μ M). 3028-KO or MES28-KO GSCs were transduced with overexpressing wild-type TNFAIP6 or mutant TNFAIP6 of K69A and K76A. Data are presented from three independent experiments. ** p < 0.01.

(J) Schematic model that illustrates co-implantation of GSCs with pTAMs into the brains of immunocompromised mice and drug administration. Created in BioRender. Wang, X. (2025) <https://BioRender.com/t65t054>.

(K–M) Representative *in vivo* bioluminescent images of NCG immunocompromised mice bearing intracranial xenografts (K). Kaplan-Meier survival curves of NCG immunocompromised mice (n = 5 for each group) are shown in (L). p values were calculated using the log-rank test. Representative images of H&E-stained coronal sections of tumor-bearing brains are shown in (M). Scale bar, 2 mm.

See also Figure S4.

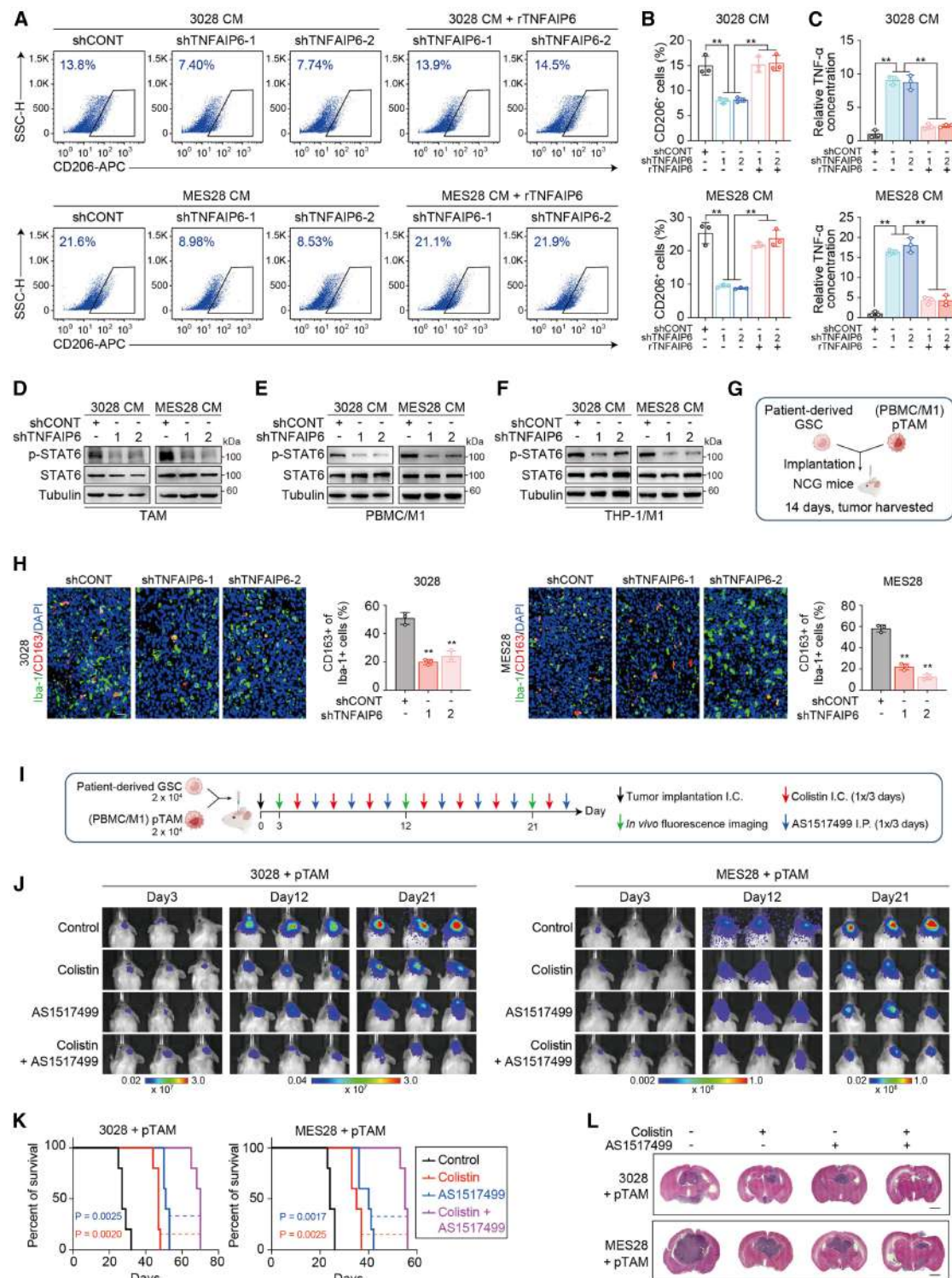


Figure 6. TNFAIP6 promotes macrophage phenotype switch from pTAMs to sTAMs

(A and B) Representative (A) and quantification (B) of flow cytometry for the percentage of CD206⁺ PBMC-induced TAM treated with CM from GSCs. Data are presented as the mean ± SEM of three independent experiments. ***p* < 0.01.

(C) ELISA quantification of TNF-α in PBMC-induced TAM. Data are presented as the mean ± SEM of three independent experiments. ***p* < 0.01.

(D–F) Immunoblot assessment of activated STAT6 (p-STAT6) protein levels in tumor-derived primary TAMs (D), PBMC- (E), and THP-1- (F) induced TAMs treated with CM from GSCs transduced with shCONT, shTNFAIP6-1, or shTNFAIP6-2.

(legend continued on next page)

favorable prognosis in KIRC but a poor prognosis in HNSC and STAD (Figures S6G and S6H).

To determine whether TNFAIP6 functions in macrophage-tumor cell interaction in HNSC and STAD, we collected an HNSC cell line, Cal27, derived from squamous cell carcinomas of the tongue, and a human gastric adenocarcinoma cell line, AGS, for the further experiments. We treated these two cell models with conditioned media from pTAMs and identified that TNFAIP6 was upregulated in the HNSC cell line (Cal27) and STAD cell line (AGS) (Figures S7A and S7B). Further, we performed the cell viability assay and found that treatment with rTNFAIP6 promoted HNSC cell line (Cal27) and STAD cell line (AGS) proliferation (Figure S7C). Mechanically, we treated HNSC cell line (Cal27) and STAD cell line (AGS) with TNFAIP6 protein (300 ng/mL), EGF (20 ng/mL), or both over a time course. TNFAIP6 alone was not able to induce p-EGFR, p-AKT, and p-mTOR in those two cell lines. By contrast, combined treatment of TNFAIP6 and EGF induced a prolonged activation of EGFR-PI3K-AKT signaling compared with EGF treatment alone (Figure S7D). In loss-of-function studies, knockdown of TNFAIP6 attenuated the activation of EGFR-PI3K-AKT signaling, supporting the vital role of TNFAIP6 in prolonging EGFR-PI3K-AKT signaling (Figures S7E and S7F). Additionally, we demonstrated that TNFAIP6 promotes macrophage phenotype switch from pTAMs to sTAMs in HNSC and STAD cell models, emphasizing its role in macrophage-tumor cell interaction (Figures S7G–S7J).

Taken together, TNFAIP6, as a pro-inflammatory stress responder, promotes GSC-associated tumor growth through binding EGF, prolonging EGFR-PI3K-AKT, and altering pTAMs to sTAMs. This shows the biological behavior of GSCs and is a promising therapeutic target for GBM.

DISCUSSION

Inflammation is an ancient, evolved process that involves the activation, recruitment, and action of the cells of innate and adaptive immunity.^{12,14} During the last couple of decades, the contribution of the immune system and inflammation to cancer development, progression, and therapy has regained enormous interest. The cellular hierarchy of GBM is generated and maintained by GSCs, which promote tumor growth, therapeutic resistance, invasion into the normal brain, immune escape, and angiogenesis.^{10,44–46} GSCs and TAMs are the important components of the GBM TME.^{47–49} Our study unveiled that pro-inflammatory stress from pTAMs maintains GSC proliferation and self-renewal, in which TNFAIP6 plays a vital role in this process. TNFAIP6 has been implicated in regulating anti-in-

flammatory functions in several diseases, including gastric cancer, brain injury, and lung injury.^{22–24} High expression of TNFAIP6 indicates a poor prognosis in GBM,²⁶ but its role between GSCs and pTAMs in GBM is unexplored. We demonstrated that TNFAIP6, induced by pTAM-derived TNF- α , maintains GSC self-renewal and tumor growth and alters macrophage phenotype from pTAMs to sTAM in GBM. Pharmacologic targeting of the molecular crosstalk between GSCs and TAMs generated sustained tumor control. Inhibition of TNFAIP6 and its downstream effectors impaired GBM tumor growth, nominating future therapeutic targets within the TME and providing additional strategies for cancer therapeutic development.

Previous studies demonstrated that TNFAIP6, as a hyaluronan (HA)-binding protein, is produced by monocytes/macrophages, mesenchymal stem cells, and fibroblasts in inflammatory diseases.^{50,51} TNFAIP6 is essential for macrophage phenotype transition in disease models such as acute lung injury.²⁴ In our studies, TNFAIP6, induced by pTAM-derived pro-inflammatory stress, prolongs EGFR-PI3K-AKT signaling activation in GSCs through EGF binding to promote GSC proliferation, demonstrating a notable node of the integrated network between tumor stem cells and neighboring macrophages.

TAMs are a prominent population of immune cells in the TME that plays an essential role in facilitating tumor progression and inducing immunosuppression.³¹ Understanding the heterogeneity and functional plasticity of TAMs is crucial for developing effective therapeutic strategies for GBM patients. Emerging evidence demonstrates that TAM populations infiltrate GBM tumors, resulting in a symbiotic interaction between distinct TAMs and tumor cells in the TME.⁵² TAMs are categorized into classically activated macrophages (M1-like phenotype) and alternatively activated macrophages (M2-like phenotype). The M1/M2 dichotomy does not represent the full complexity of TAMs in GBM.^{53,54} In this study, we identified TNFAIP6 as a responder in GSCs to pTAM stress, which activates M2-like/anti-inflammatory macrophages (sTAMs). GSCs recruit TAMs through the secretion of chemoattractants and promote an M2-like phenotype.^{31,55} TAMs maintain GSCs and facilitate GBM progression and therapeutic resistance.^{56,57} Therefore, molecular crosstalk between GSCs and TAMs is bidirectional, promoting the collaborative maintenance of the immunosuppressive TME in GBM.

EGFR activation is one of the most important derangements in GBM, with over half of all GBM patients harboring a mutation, rearrangement, splicing alteration, or amplification of EGFR.^{58,59} Overexpression or mutations of EGFR are recurrent molecular alterations in GBM associated with an unfavorable prognosis.⁶⁰

(G) Schematic model that illustrates co-implantation of patient-derived GSCs with pTAMs into the brains of immunocompromised mice. Tumors were harvested after 14 days. Created in BioRender. Wang, X. (2025) <https://BioRender.com/t65t054>.

(H) Immunofluorescent staining of CD163 (green) and the pan-macrophage marker Iba1 (red) in GBM xenografts derived from GSCs expressing shCONT or shTNFAIP6. Scale bar, 20 μ m.

(I) Schematic model that illustrates co-implantation of GSCs with pTAMs into the brains of immunocompromised mice and drug administration. Created in BioRender. Wang, X. (2025) <https://BioRender.com/t65t054>.

(J–L) Representative *in vivo* bioluminescent images of NCG immunocompromised mice bearing intracranial xenografts (J). Kaplan-Meier survival curves of NCG immunocompromised mice ($n = 5$ for each group) are shown in (K). p values were calculated using the log-rank test. Representative images of H&E-stained coronal sections of tumor-bearing brains are shown in (L). Scale bar, 2 mm.

See also Figure S5.

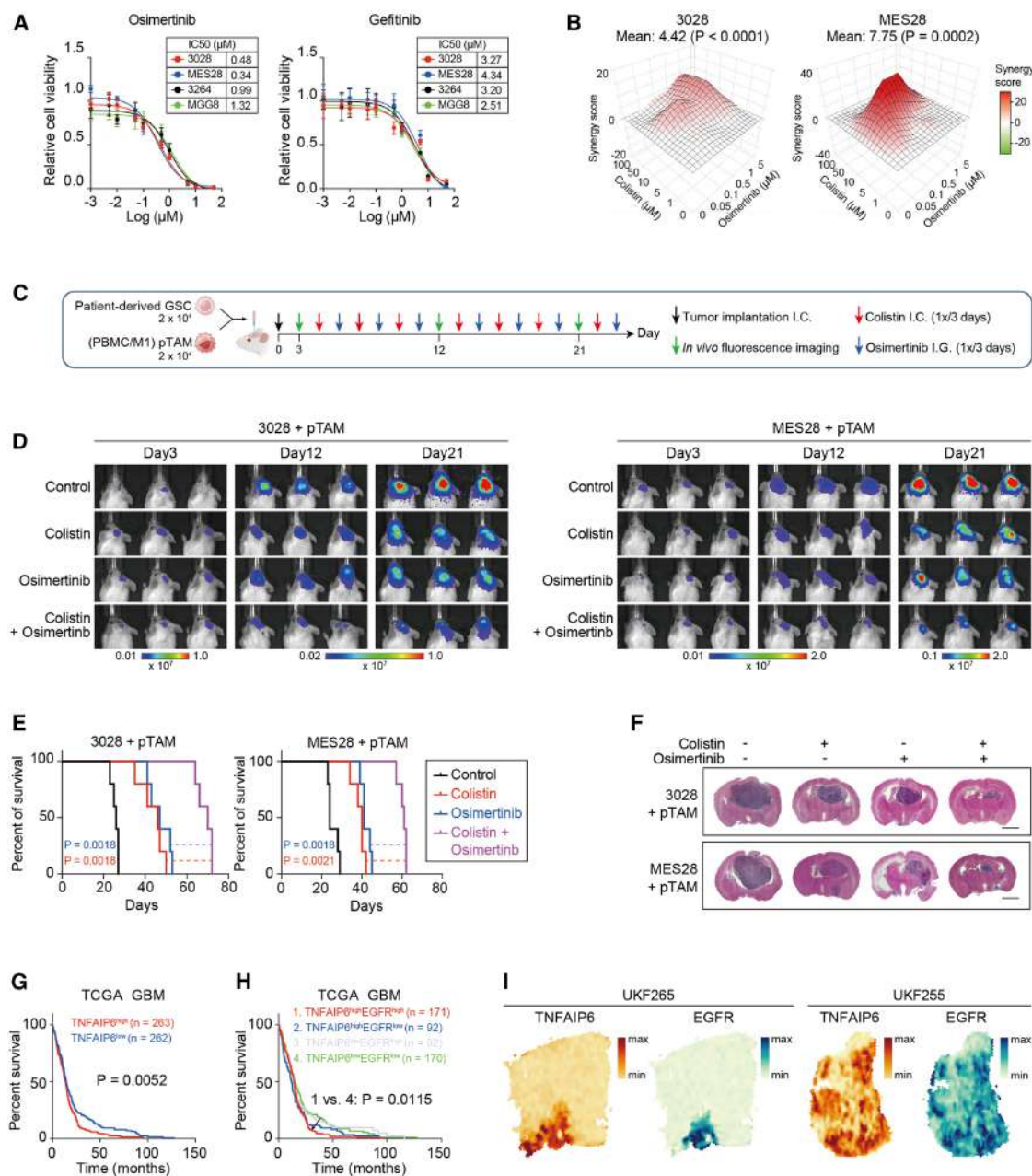


Figure 7. Pharmacologic targeting of TNFAIP6 augments anti-tumor efficacy of EGFR inhibition in GBM

(A) Dose-response curves for EGFR inhibitors, gefitinib or osimertinib, in four patient-derived GSC models.

(B) Calculation and visualization of synergy scores for drug combinations of osimertinib and colistin.

(C) Schematic model that illustrates co-implantation of GSCs with pTAMs into the brains of immunocompromised mice and drug administration. Created in BioRender. Wang, X. (2025) <https://BioRender.com/t65t054>.

(D–F) Representative *in vivo* bioluminescent images of NCG immunocompromised mice bearing intracranial xenografts (D). Kaplan-Meier survival curves of NCG immunocompromised mice (n = 5 for each group) are shown in (E). P values were calculated using the log-rank test. Representative images of H&E-stained coronal sections of tumor-bearing brains are shown in (F). Scale bar, 2 mm.

(G and H) Interrogation of the TCGA GBM dataset indicates a negative correlation between the expression of TNFAIP6 (G) and TNFAIP6 combined with EGFR (H).

(I) Examples of spatial expression patterns of EGFR and TNFAIP6.

See also Figures S6 and S7.

Clinical trials targeting EGFR therapy have proven ineffective in treating patients with GBM, even in combination with temozolomide.⁶¹ Our data suggested that the lack of effectiveness for

EGFR inhibitors may be partially attributed to the signaling maintenance in GBM. Osimertinib is a third-generation tyrosine kinase inhibitor that irreversibly inhibits EGFR but penetrates the

blood-brain barrier more effectively than other inhibitors.^{62,63} TNFAIP6-EGF binding maintains GSCs by prolonging EGFR-PI3K-AKT signaling activation. Targeting EGFR signaling combined with TNFAIP6-EGF blockade may represent a promising strategy to inhibit the EGFR activation and maintenance mechanisms in tumor malignant progression.

In conclusion, our study identified TNFAIP6 as a responder in GSCs to pro-inflammatory stress TNF- α from pTAMs, promoting GSC-associated tumor growth through binding EGF and prolonging EGFR-PI3K-AKT signaling activation. Meanwhile, pro-inflammatory stress-induced GSCs secrete TNFAIP6 to induce phenotype transformation of pTAMs to sTAMs. TNFAIP6 plays both autocrine and paracrine roles in maintaining the immunosuppressive TME. The pharmacological disruption of TNFAIP6 and STAT6 or EGFR effectively suppresses GBM growth, informing a combinatorial targeting strategy that will advance the therapeutic development against GBM. Considering the role of GSCs in the tumor ecosystem and the limited efficacy of GSC-targeted monotherapy, the disruption of GSC-oncogenic signaling in combination with targeting TAM dependencies will improve our understanding of dynamics in the TME, which may provide a promising therapeutic rationale for GBM patients.

Limitations of the study

This study has identified that pro-inflammatory stress TNF- α from pTAMs induces TNFAIP6 and promotes GSC-associated tumor growth; however, it is possible that other pro-inflammatory cytokines could mediate the complex tumor-immune interaction and contribute to GBM progression. In addition, further prospective investigations with clinical validation are required to confirm the therapeutic benefit of colistin, the drug that targets the TNFAIP6-EGF binding residues, as a treatment approach for GBM.

RESOURCE AVAILABILITY

Lead contact

Requests for further information and resources should be directed to and will be fulfilled by the lead contact, Dr. Xiuxing Wang (drxiuxingwang@163.com).

Materials availability

This study did not generate new, unique reagents.

Data and code availability

- The processed data generated for this study can be obtained upon request from the [lead contact](#).
- This study did not generate new code.
- Raw GBM scRNA-seq data derived from human samples have been deposited at the GSA database, in the Genome Sequence Archive in the National Genomics Data Center China National Center, the China National Center for Bioinformation/Beijing Institute of Genomics, and the Chinese Academy of Sciences,^{64,65} and the accession number is listed in the [key resources table](#). Local law prohibits depositing raw GBM scRNA-seq datasets derived from human samples outside of the country of origin. Prior to publication, the authors officially requested that the raw scRNA-seq data datasets reported in this paper be made publicly accessible. To request access, contact the [lead contact](#).
- Any additional information required to reanalyze the data reported in this work paper is available from the [lead contact](#) upon request.

ACKNOWLEDGMENTS

We thank the Nanjing Medical University Analysis Center for help with fluorescence-activated cell sorting (FACS) and the animal core facility of Nanjing Medical University for help with animal experiments. This work was supported by the National Natural Science Foundation of China (82072779 to X.W. and 82403427 to D.G.), the Jiangsu Provincial Key Research Development Program of China (BE2022770 to Y.C.), and the China Postdoctoral Science Foundation (2023M741795 to D.G.). Kailin Yang was supported by the Computational Genomic Epidemiology of Cancer (CoGEC) Program at Case Comprehensive Cancer Center (T32CA094186), the Young Investigator Award in Glioblastoma from the ASCO Conquer Cancer Foundation, and the RSNA Research Fellow Grant. Kun Yang was supported by the Research Personnel Cultivation Programme of Zhongda Hospital, Southeast University (CZXM-GSP-RC-152), Zhongda Hospital Affiliated to Southeast University, the Jiangsu Province High-Level Hospital Pairing Assistance Construction Funds (zdlyg05), and the Medical Science and Technology Development Foundation of Nanjing (ZKX22041).

AUTHOR CONTRIBUTIONS

D.G., L.H., W.Y., D.S., and J.G. performed all experiments, analyzed data, and prepared figures, with help from J. Li. D.G., Kailin Yang, and J.G. contributed to the design of the study and wrote the manuscript, with help from R.C.G., D.D., Z.Z., D.L., Q. Wu, and N. Zhao. Z.S., Y.W., Kun Yang, J.S., F.L., Q. Wang, G.J., Y.C., and X.Q. provided resources. Z.H., C.L., N. Zhang, and Y.Y. provided key scientific inputs. D.G., Kailin Yang, Kun Yang, Y.C., and X.W. acquired funding. J. Liu, Q.Z., J.Z., J.N.R., and X.W. conceptualized and coordinated the study, analyzed the data, and edited the paper. All authors read and edited the manuscript.

DECLARATION OF INTERESTS

The authors declare no competing interests.

STAR★METHODS

Detailed methods are provided in the online version of this paper and include the following:

- [KEY RESOURCES TABLE](#)
- [EXPERIMENTAL MODEL AND STUDY PARTICIPANT DETAILS](#)
 - Patients and human tumor samples
 - Patient-derived and cell line models
 - Mice
- [METHOD DETAILS](#)
 - Isolation and differentiation of PBMC
 - Differentiation of THP-1 cells
 - *In vivo* tumorigenesis
 - Spatial transcriptomics data processing
 - Single-cell RNA analysis
 - Signaling signature analysis
 - Lentiviral production and transfection
 - Cell proliferation assay
 - Neurosphere formation assay
 - Quantitative RT-PCR
 - Western blotting
 - Co-immunoprecipitation
 - Flow Cytometry Analysis
 - Immunofluorescence
 - Immunohistochemistry
 - Molecular docking
 - Surface plasmon resonance (SPR)
 - Bio-Layer Interferometry (BLI)
 - *In vivo* drug treatment
 - *In vivo* bioluminescence analysis
- [QUANTIFICATION AND STATISTICAL ANALYSIS](#)

SUPPLEMENTAL INFORMATION

Supplemental information can be found online at <https://doi.org/10.1016/j.devcel.2025.04.027>.

Received: August 20, 2024

Revised: January 21, 2025

Accepted: April 30, 2025

Published: May 21, 2025

REFERENCES

1. Tan, A.C., Ashley, D.M., López, G.Y., Malinzak, M., Friedman, H.S., and Khasraw, M. (2020). Management of glioblastoma: State of the art and future directions. *CA Cancer J. Clin.* 70, 299–312. <https://doi.org/10.3322/caac.21613>.
2. Perry, J.R., Laperriere, N., O'Callaghan, C.J., Brandes, A.A., Menten, J., Phillips, C., Fay, M., Nishikawa, R., Cairncross, J.G., Roa, W., et al. (2017). Short-Course Radiation plus Temozolomide in Elderly Patients with Glioblastoma. *N. Engl. J. Med.* 376, 1027–1037. <https://doi.org/10.1056/NEJMoa1611977>.
3. Wakimoto, H., Kesari, S., Farrell, C.J., Curry, W.T., Jr., Zaupa, C., Aghi, M., Kuroda, T., Stemmer-Rachamimov, A., Shah, K., Liu, T.C., et al. (2009). Human glioblastoma-derived cancer stem cells: establishment of invasive glioma models and treatment with oncolytic herpes simplex virus vectors. *Cancer Res.* 69, 3472–3481. <https://doi.org/10.1158/0008-5472.Can-08-3886>.
4. Sarkar, S., Döring, A., Zemp, F.J., Silva, C., Lun, X., Wang, X., Kelly, J., Hader, W., Hamilton, M., Mercier, P., et al. (2014). Therapeutic activation of macrophages and microglia to suppress brain tumor-initiating cells. *Nat. Neurosci.* 17, 46–55. <https://doi.org/10.1038/nn.3597>.
5. Bao, S., Wu, Q., Sathornsumetee, S., Hao, Y., Li, Z., Hjelmeland, A.B., Shi, Q., McLendon, R.E., Bigner, D.D., and Rich, J.N. (2006). Stem cell-like glioma cells promote tumor angiogenesis through vascular endothelial growth factor. *Cancer Res.* 66, 7843–7848. <https://doi.org/10.1158/0008-5472.Can-06-1010>.
6. Bao, S., Wu, Q., McLendon, R.E., Hao, Y., Shi, Q., Hjelmeland, A.B., Dewhirst, M.W., Bigner, D.D., and Rich, J.N. (2006). Glioma stem cells promote radioresistance by preferential activation of the DNA damage response. *Nature* 444, 756–760. <https://doi.org/10.1038/nature05236>.
7. Wu, L., Zhao, Z., Shin, Y.J., Yin, Y., Raju, A., Vaiyapuri, T.S., Idzham, K., Son, M., Lee, Y., Sa, J.K., et al. (2024). Tumour microenvironment programming by an RNA-RNA-binding protein complex creates a druggable vulnerability in IDH-wild-type glioblastoma. *Nat. Cell Biol.* 26, 1003–1018. <https://doi.org/10.1038/s41556-024-01428-5>.
8. Chen, J., McKay, R.M., and Parada, L.F. (2012). Malignant glioma: lessons from genomics, mouse models, and stem cells. *Cell* 149, 36–47. <https://doi.org/10.1016/j.cell.2012.03.009>.
9. Gimple, R.C., Yang, K., Halbert, M.E., Agnihotri, S., and Rich, J.N. (2022). Brain cancer stem cells: resilience through adaptive plasticity and hierarchical heterogeneity. *Nat. Rev. Cancer* 22, 497–514. <https://doi.org/10.1038/s41568-022-00486-x>.
10. Prager, B.C., Xie, Q., Bao, S., and Rich, J.N. (2019). Cancer Stem Cells: The Architects of the Tumor Ecosystem. *Cell Stem Cell* 24, 41–53. <https://doi.org/10.1016/j.stem.2018.12.009>.
11. Singh, S.K., Hawkins, C., Clarke, I.D., Squire, J.A., Bayani, J., Hide, T., Henkelman, R.M., Cusimano, M.D., and Dirks, P.B. (2004). Identification of human brain tumour initiating cells. *Nature* 429, 396–401. <https://doi.org/10.1038/nature03128>.
12. Medzhitov, R. (2008). Origin and physiological roles of inflammation. *Nature* 454, 428–435. <https://doi.org/10.1038/nature07201>.
13. Hoekstra, M.E., Slagter, M., Urbanus, J., Toebes, M., Slingerland, N., de Rink, I., Kluin, R.J.C., Nieuwland, M., Kerkhoven, R., Wessels, L.F.A., et al. (2024). Distinct spatiotemporal dynamics of CD8+ T cell-derived cytokines in the tumor microenvironment. *Cancer Cell* 42, 157–167.e9. <https://doi.org/10.1016/j.ccell.2023.12.010>.
14. Greten, F.R., and Grivennikov, S.I. (2019). Inflammation and Cancer: Triggers, Mechanisms, and Consequences. *Immunity* 51, 27–41. <https://doi.org/10.1016/j.immuni.2019.06.025>.
15. Verfaillie, T., Garg, A.D., and Agostinis, P. (2013). Targeting ER stress induced apoptosis and inflammation in cancer. *Cancer Lett.* 332, 249–264. <https://doi.org/10.1016/j.canlet.2010.07.016>.
16. Berg, T.J., Marques, C., Pantazopoulou, V., Johansson, E., von Stedingk, K., Lindgren, D., Jeannot, P., Pietras, E.J., Bergström, T., Swartling, F.J., et al. (2021). The Irradiated Brain Microenvironment Supports Glioma Stemness and Survival via Astrocyte-Derived Transglutaminase 2. *Cancer Res.* 81, 2101–2115. <https://doi.org/10.1158/0008-5472.Can-20-1785>.
17. Dapash, M., Hou, D., Castro, B., Lee-Chang, C., and Lesniak, M.S. (2021). The Interplay between Glioblastoma and Its Microenvironment. *Cells* 10, 2257. <https://doi.org/10.3390/cells10092257>.
18. Gimple, R.C., Bhargava, S., Dixit, D., and Rich, J.N. (2019). Glioblastoma stem cells: lessons from the tumor hierarchy in a lethal cancer. *Genes Dev.* 33, 591–609. <https://doi.org/10.1101/gad.324301.119>.
19. Li, J., Wang, K., Yang, C., Zhu, K., Jiang, C., Wang, M., Zhou, Z., Tang, N., Wang, Q., Wang, S., et al. (2023). Tumor-Associated Macrophage-Derived Exosomal LINC01232 Induces the Immune Escape in Glioma by Decreasing Surface MHC-I Expression. *Adv. Sci. (Weinh)* 10, e2207067. <https://doi.org/10.1002/adv.202207067>.
20. Cassetta, L., and Pollard, J.W. (2023). A timeline of tumour-associated macrophage biology. *Nat. Rev. Cancer* 23, 238–257. <https://doi.org/10.1038/s41568-022-00547-1>.
21. Yuan, W., Zhang, Q., Gu, D., Lu, C., Dixit, D., Gimple, R.C., Gao, Y., Gao, J., Li, D., Shan, D., et al. (2023). Dual Role of CXCL8 in Maintaining the Mesenchymal State of Glioblastoma Stem Cells and M2-Like Tumor-Associated Macrophages. *Clin. Cancer Res.* 29, 3779–3792. <https://doi.org/10.1158/1078-0432.CCR-22-3273>.
22. Zhang, X., Xue, J., Yang, H., Zhou, T., and Zu, G. (2021). TNFAIP6 promotes invasion and metastasis of gastric cancer and indicates poor prognosis of patients. *Tissue Cell* 68, 101455. <https://doi.org/10.1016/j.tice.2020.101455>.
23. Day, A.J., and Milner, C.M. (2019). TSG-6: A multifunctional protein with anti-inflammatory and tissue-protective properties. *Matrix Biol.* 78–79, 60–83. <https://doi.org/10.1016/j.matbio.2018.01.011>.
24. Mittal, M., Tirupathi, C., Nepal, S., Zhao, Y.Y., Grzych, D., Soni, D., Prockop, D.J., and Malik, A.B. (2016). TNF α -stimulated gene-6 (TSG6) activates macrophage phenotype transition to prevent inflammatory lung injury. *Proc. Natl. Acad. Sci. USA* 113, E8151–E8158. <https://doi.org/10.1073/pnas.1614935113>.
25. Yang, H., Wu, L., Deng, H., Chen, Y., Zhou, H., Liu, M., Wang, S., Zheng, L., Zhu, L., and Lv, X. (2020). Anti-inflammatory protein TSG-6 secreted by bone marrow mesenchymal stem cells attenuates neuropathic pain by inhibiting the TLR2/MyD88/NF- κ B signaling pathway in spinal microglia. *J. Neuroinflammation* 17, 154. <https://doi.org/10.1186/s12974-020-1731-x>.
26. Lin, D., Li, W., Zhang, N., and Cai, M. (2022). Identification of TNFAIP6 as a hub gene associated with the progression of glioblastoma by weighted gene co-expression network analysis. *IET Syst. Biol.* 16, 145–156. <https://doi.org/10.1049/syb2.12046>.
27. Puchalski, R.B., Shah, N., Miller, J., Dalley, R., Nomura, S.R., Yoon, J.G., Smith, K.A., Lankovich, M., Bertagnolli, D., Bickley, K., et al. (2018). An anatomic transcriptional atlas of human glioblastoma. *Science* 360, 660–663. <https://doi.org/10.1126/science.aaf2666>.
28. Ravi, V.M., Will, P., Kueckelhaus, J., Sun, N., Joseph, K., Salié, H., Vollmer, L., Kuliesiute, U., von Ehr, J., Benotmane, J.K., et al. (2022). Spatially resolved multi-omics deciphers bidirectional tumor-host interdependence in glioblastoma. *Cancer Cell* 40, 639–655.e13. <https://doi.org/10.1016/j.ccell.2022.05.009>.

29. Abdelfattah, N., Kumar, P., Wang, C., Leu, J.S., Flynn, W.F., Gao, R., Baskin, D.S., Pichumani, K., Ijare, O.B., Wood, S.L., et al. (2022). Single-cell analysis of human glioma and immune cells identifies S100A4 as an immunotherapy target. *Nat. Commun.* **13**, 767. <https://doi.org/10.1038/s41467-022-28372-y>.
30. Wang, L.B., Karpova, A., Gritsenko, M.A., Kyle, J.E., Cao, S., Li, Y., Rykunov, D., Colaprico, A., Rothstein, J.H., Hong, R., et al. (2021). Proteogenomic and metabolomic characterization of human glioblastoma. *Cancer Cell* **39**, 509–528.e20. <https://doi.org/10.1016/j.ccell.2021.01.006>.
31. Shi, Y., Ping, Y.F., Zhou, W., He, Z.C., Chen, C., Bian, B.S.J., Zhang, L., Chen, L., Lan, X., Zhang, X.C., et al. (2017). Tumour-associated macrophages secrete pleiotrophin to promote PTPRZ1 signalling in glioblastoma stem cells for tumour growth. *Nat. Commun.* **8**, 15080. <https://doi.org/10.1038/ncomms15080>.
32. Zhai, K., Huang, Z., Huang, Q., Tao, W., Fang, X., Zhang, A., Li, X., Stark, G.R., Hamilton, T.A., and Bao, S. (2021). Pharmacological inhibition of BACE1 suppresses glioblastoma growth by stimulating macrophage phagocytosis of tumor cells. *Nat. Cancer* **2**, 1136–1151. <https://doi.org/10.1038/s43018-021-00267-9>.
33. Cancer; Genome; Atlas; Research Network, Weinstein, J.N., Collisson, E. A., Mills, G.B., Shaw, K.R.M., Ozenberger, B.A., Ellrott, K., Shmulevich, I., Sander, C., and Stuart, J.M. (2013). The Cancer Genome Atlas Pan-Cancer analysis project. *Nat. Genet.* **45**, 1113–1120. <https://doi.org/10.1038/ng.2764>.
34. Mack, S.C., Singh, I., Wang, X., Hirsch, R., Wu, Q., Villagomez, R., Bernatchez, J.A., Zhu, Z., Gimple, R.C., Kim, L.J.Y., et al. (2019). Chromatin landscapes reveal developmentally encoded transcriptional states that define human glioblastoma. *J. Exp. Med.* **216**, 1071–1090. <https://doi.org/10.1084/jem.20190196>.
35. Suvà, M.L., Rheinbay, E., Gillespie, S.M., Patel, A.P., Wakimoto, H., Rabkin, S.D., Riggi, N., Chi, A.S., Cahill, D.P., Nahed, B.V., et al. (2014). Reconstructing and reprogramming the tumor-propagating potential of glioblastoma stem-like cells. *Cell* **157**, 580–594. <https://doi.org/10.1016/j.cell.2014.02.030>.
36. Wang, M., Chen, S., He, X., Yuan, Y., and Wei, X. (2024). Targeting inflammation as cancer therapy. *J. Hematol. Oncol.* **17**, 13. <https://doi.org/10.1186/s13045-024-01528-7>.
37. Olivera, I., Sanz-Pamplona, R., Bolaños, E., Rodríguez, I., Etxeberria, I., Cirella, A., Egea, J., Garasa, S., Migueliz, I., Eguren-Santamaria, I., et al. (2022). A Therapeutically Actionable Protumoral Axis of Cytokines Involving IL-8, TNF α , and IL-1 β . *Cancer Discov.* **12**, 2140–2157. <https://doi.org/10.1158/2159-8290.CD-21-1115>.
38. Kusne, Y., Carrera-Silva, E.A., Perry, A.S., Rushing, E.J., Mandell, E.K., Dietrich, J.D., Errasti, A.E., Gibbs, D., Berens, M.E., Loftus, J.C., et al. (2014). Targeting aPKC disables oncogenic signaling by both the EGFR and the proinflammatory cytokine TNF α in glioblastoma. *Sci. Signal.* **7**, ra75. <https://doi.org/10.1126/scisignal.2005196>.
39. Kozakov, D., Hall, D.R., Xia, B., Porter, K.A., Padhorny, D., Yueh, C., Beglov, D., and Vajda, S. (2017). The ClusPro web server for protein-protein docking. *Nat. Protoc.* **12**, 255–278. <https://doi.org/10.1038/nprot.2016.169>.
40. El-Sayed Ahmed, M.A.E., Zhong, L.L., Shen, C., Yang, Y., Doi, Y., and Tian, G.B. (2020). Colistin and its role in the Era of antibiotic resistance: an extended review (2000–2019). *Emerg. Microbes Infect.* **9**, 868–885. <https://doi.org/10.1080/22221751.2020.1754133>.
41. Lee, R.H., Yu, J.M., Foskett, A.M., Peltier, G., Reneau, J.C., Bazhanov, N., Oh, J.Y., and Prockop, D.J. (2014). TSG-6 as a biomarker to predict efficacy of human mesenchymal stem/progenitor cells (hMSCs) in modulating sterile inflammation in vivo. *Proc. Natl. Acad. Sci. USA* **111**, 16766–16771. <https://doi.org/10.1073/pnas.1416121111>.
42. Johnson, K.C., Anderson, K.J., Courtois, E.T., Gujar, A.D., Barthel, F.P., Varn, F.S., Luo, D., Seignon, M., Yi, E., Kim, H., et al. (2021). Single-cell multimodal glioma analyses identify epigenetic regulators of cellular plasticity and environmental stress response. *Nat. Genet.* **53**, 1456–1468. <https://doi.org/10.1038/s41588-021-00926-8>.
43. Bowman, R.L., Wang, Q., Carro, A., Verhaak, R.G.W., and Squatrito, M. (2017). Gliovis data portal for visualization and analysis of brain tumor expression datasets. *Neuro. Oncol.* **19**, 139–141. <https://doi.org/10.1093/neuonc/now247>.
44. Moore, K.A., and Lemischka, I.R. (2006). Stem cells and their niches. *Science* **311**, 1880–1885. <https://doi.org/10.1126/science.1110542>.
45. Alvarado, A.G., Thiagarajan, P.S., Mulkearns-Hubert, E.E., Silver, D.J., Hale, J.S., Alban, T.J., Turaga, S.M., Jarrar, A., Reizes, O., Longworth, M.S., et al. (2017). Glioblastoma Cancer Stem Cells Evade Innate Immune Suppression of Self-Renewal through Reduced TLR4 Expression. *Cell Stem Cell* **20**, 450–461.e4. <https://doi.org/10.1016/j.stem.2016.12.001>.
46. Lathia, J.D., Mack, S.C., Mulkearns-Hubert, E.E., Valentim, C.L.L., and Rich, J.N. (2015). Cancer stem cells in glioblastoma. *Genes Dev.* **29**, 1203–1217. <https://doi.org/10.1101/gad.261982.115>.
47. Chen, P., Hsu, W.H., Chang, A., Tan, Z., Lan, Z., Zhou, A., Spring, D.J., Lang, F.F., Wang, Y.A., and DePinho, R.A. (2020). Circadian Regulator CLOCK Recruits Immune-Suppressive Microglia into the GBM Tumor Microenvironment. *Cancer Discov.* **10**, 371–381. <https://doi.org/10.1158/2159-8290.CD-19-0400>.
48. Tao, W., Chu, C., Zhou, W., Huang, Z., Zhai, K., Fang, X., Huang, Q., Zhang, A., Wang, X., Yu, X., et al. (2020). Dual Role of WISP1 in maintaining glioma stem cells and tumor-supportive macrophages in glioblastoma. *Nat. Commun.* **11**, 3015. <https://doi.org/10.1038/s41467-020-16827-z>.
49. Yin, J., Kim, S.S., Choi, E., Oh, Y.T., Lin, W., Kim, T.H., Sa, J.K., Hong, J.H., Park, S.H., Kwon, H.J., et al. (2020). ARS2/MAGL signaling in glioblastoma stem cells promotes self-renewal and M2-like polarization of tumor-associated macrophages. *Nat. Commun.* **11**, 2978. <https://doi.org/10.1038/s41467-020-16789-2>.
50. Yu, Q., Zhang, S., Wang, H., Zhang, Y., Feng, T., Chen, B., He, Y., Zeng, Z., and Chen, M. (2016). TNFAIP6 is a potential biomarker of disease activity in inflammatory bowel disease. *Biomark. Med.* **10**, 473–483. <https://doi.org/10.2217/bmm.16.9>.
51. Wisniewski, H.G., and Vilcek, J. (2004). Cytokine-induced gene expression at the crossroads of innate immunity, inflammation and fertility: TSG-6 and PTX3/TSG-14. *Cytokine Growth Factor Rev.* **15**, 129–146. <https://doi.org/10.1016/j.cytogfr.2004.01.005>.
52. Xuan, W., Hsu, W.H., Khan, F., Dunterman, M., Pang, L., Wainwright, D.A., Ahmed, A.U., Heimberger, A.B., Lesniak, M.S., and Chen, P. (2022). Circadian Regulator CLOCK Drives Immunosuppression in Glioblastoma. *Cancer Immunol. Res.* **10**, 770–784. <https://doi.org/10.1158/2326-6066.CIR-21-0559>.
53. Khan, F., Pang, L., Dunterman, M., Lesniak, M.S., Heimberger, A.B., and Chen, P. (2023). Macrophages and microglia in glioblastoma: heterogeneity, plasticity, and therapy. *J. Clin. Invest.* **133**, e163446. <https://doi.org/10.1172/JCI163446>.
54. Xuan, W., Lesniak, M.S., James, C.D., Heimberger, A.B., and Chen, P. (2021). Context-Dependent Glioblastoma-Macrophage/Microglia Symbiosis and Associated Mechanisms. *Trends Immunol.* **42**, 280–292. <https://doi.org/10.1016/j.it.2021.02.004>.
55. Wu, A., Wei, J., Kong, L.Y., Wang, Y., Priebe, W., Qiao, W., Sawaya, R., and Heimberger, A.B. (2010). Glioma cancer stem cells induce immunosuppressive macrophages/microglia. *Neuro-Oncology* **12**, 1113–1125. <https://doi.org/10.1093/neuonc/noon082>.
56. Yan, J., Zhao, Q., Wang, J., Tian, X., Wang, J., Xia, X., Ott, M., Rao, G., Heimberger, A.B., and Li, S. (2021). FGL2-wired macrophages secrete CXCL7 to regulate the stem-like functionality of glioma cells. *Cancer Lett.* **506**, 83–94. <https://doi.org/10.1016/j.canlet.2021.02.021>.
57. Bloch, O., Crane, C.A., Kaur, R., Safaee, M., Rutkowski, M.J., and Parsa, A.T. (2013). Gliomas promote immunosuppression through induction of B7-H1 expression in tumor-associated macrophages. *Clin. Cancer Res.* **19**, 3165–3175. <https://doi.org/10.1158/1078-0432.CCR-12-3314>.

58. An, Z., Aksoy, O., Zheng, T., Fan, Q.W., and Weiss, W.A. (2018). Epidermal growth factor receptor and EGFRvIII in glioblastoma: signaling pathways and targeted therapies. *Oncogene* 37, 1561–1575. <https://doi.org/10.1038/s41388-017-0045-7>.
59. Hu, C., Leche, C.A., 2nd, Kiyatkin, A., Yu, Z., Stayrook, S.E., Ferguson, K. M., and Lemmon, M.A. (2022). Glioblastoma mutations alter EGFR dimer structure to prevent ligand bias. *Nature* 602, 518–522. <https://doi.org/10.1038/s41586-021-04393-3>.
60. Eskilsson, E., Røslund, G.V., Solecki, G., Wang, Q., Harter, P.N., Graziani, G., Verhaak, R.G.W., Winkler, F., Bjerkvig, R., and Miletic, H. (2018). EGFR heterogeneity and implications for therapeutic intervention in glioblastoma. *Neuro-Oncology* 20, 743–752. <https://doi.org/10.1093/neuonc/nox191>.
61. Meng, X., Zhao, Y., Han, B., Zha, C., Zhang, Y., Li, Z., Wu, P., Qi, T., Jiang, C., Liu, Y., et al. (2020). Dual functionalized brain-targeting nanoinhibitors restrain temozolomide-resistant glioma via attenuating EGFR and MET signaling pathways. *Nat. Commun.* 11, 594. <https://doi.org/10.1038/s41467-019-14036-x>.
62. Makhlin, I., Salinas, R.D., Zhang, D., Jacob, F., Ming, G.L., Song, H., Saxena, D., Dorsey, J.F., Nasrallah, M.P., Morrisette, J.J., et al. (2019). Clinical activity of the EGFR tyrosine kinase inhibitor osimertinib in EGFR-mutant glioblastoma. *CNS Oncol.* 8, CNS43. <https://doi.org/10.2217/cns-2019-0014>.
63. Leonetti, A., Sharma, S., Minari, R., Perego, P., Giovannetti, E., and Tiseo, M. (2019). Resistance mechanisms to osimertinib in EGFR-mutated non-small cell lung cancer. *Br. J. Cancer* 121, 725–737. <https://doi.org/10.1038/s41416-019-0573-8>.
64. Chen, T., Chen, X., Zhang, S., Zhu, J., Tang, B., Wang, A., Dong, L., Zhang, Z., Yu, C., Sun, Y., et al. (2021). The Genome Sequence Archive Family: Toward Explosive Data Growth and Diverse Data Types. *Genomics Proteomics Bioinformatics* 19, 578–583. <https://doi.org/10.1016/j.gpb.2021.08.001>.
65. CNCB-NGDC Members and Partners (2024). Database Resources of the National Genomics Data Center, China National Center for Bioinformatics in 2024. *Nucleic Acids Res.* 52, D18–D32. <https://doi.org/10.1093/nar/gkad1078>.
66. Stewart, S.A., Dykxhoorn, D.M., Palliser, D., Mizuno, H., Yu, E.Y., An, D.S., Sabatini, D.M., Chen, I.S.Y., Hahn, W.C., Sharp, P.A., et al. (2003). Lentivirus-delivered stable gene silencing by RNAi in primary cells. *RNA* 9, 493–501. <https://doi.org/10.1261/rna.2192803>.
67. Korsunsky, I., Millard, N., Fan, J., Slowikowski, K., Zhang, F., Wei, K., Baglaenko, Y., Brenner, M., Loh, P.R., and Raychaudhuri, S. (2019). Fast, sensitive and accurate integration of single-cell data with Harmony. *Nat. Methods* 16, 1289–1296. <https://doi.org/10.1038/s41592-019-0619-0>.
68. Satija, R., Farrell, J.A., Gennert, D., Schier, A.F., and Regev, A. (2015). Spatial reconstruction of single-cell gene expression data. *Nat. Biotechnol.* 33, 495–502. <https://doi.org/10.1038/nbt.3192>.
69. Hänzelmann, S., Castelo, R., and Guinney, J. (2013). GSVA: gene set variation analysis for microarray and RNA-seq data. *BMC Bioinformatics* 14, 7. <https://doi.org/10.1186/1471-2105-14-7>.
70. Pang, L., Dunterman, M., Guo, S., Khan, F., Liu, Y., Taefi, E., Bahrami, A., Geula, C., Hsu, W.H., Horbinski, C., et al. (2023). Kunitz-type protease inhibitor TFPI2 remodels stemness and immunosuppressive tumor microenvironment in glioblastoma. *Nat. Immunol.* 24, 1654–1670. <https://doi.org/10.1038/s41590-023-01605-y>.
71. Miranda, A., Hamilton, P.T., Zhang, A.W., Pattnaik, S., Becht, E., Mezheyeuski, A., Bruun, J., Micke, P., de Reynies, A., and Nelson, B.H. (2019). Cancer stemness, intratumoral heterogeneity, and immune response across cancers. *Proc. Natl. Acad. Sci. USA* 116, 9020–9029. <https://doi.org/10.1073/pnas.1818210116>.
72. Subramanian, A., Tamayo, P., Mootha, V.K., Mukherjee, S., Ebert, B.L., Gillette, M.A., Paulovich, A., Pomeroy, S.L., Golub, T.R., Lander, E.S., and Mesirov, J.P. (2005). Gene set enrichment analysis: a knowledge-based approach for interpreting genome-wide expression profiles. *Proc. Natl. Acad. Sci. USA* 102, 15545–15550. <https://doi.org/10.1073/pnas.0506580102>.
73. Mootha, V.K., Lindgren, C.M., Eriksson, K.F., Subramanian, A., Sihag, S., Lehar, J., Puigserver, P., Carlsson, E., Ridderstråle, M., Laurila, E., et al. (2003). PGC-1alpha-responsive genes involved in oxidative phosphorylation are coordinately downregulated in human diabetes. *Nat. Genet.* 34, 267–273. <https://doi.org/10.1038/ng1180>.
74. Flavahan, W.A., Wu, Q., Hitomi, M., Rahim, N., Kim, Y., Sloan, A.E., Weil, R.J., Nakano, I., Sarkaria, J.N., Stringer, B.W., et al. (2013). Brain tumor initiating cells adapt to restricted nutrition through preferential glucose uptake. *Nat. Neurosci.* 16, 1373–1382. <https://doi.org/10.1038/nn.3510>.
75. Hu, Y., and Smyth, G.K. (2009). ELDA: extreme limiting dilution analysis for comparing depleted and enriched populations in stem cell and other assays. *J. Immunol. Methods* 347, 70–78. <https://doi.org/10.1016/j.jim.2009.06.008>.

STAR★METHODS

KEY RESOURCES TABLE

REAGENT or RESOURCE	SOURCE	IDENTIFIER
Antibodies		
Human TruStain FcX™ (Fc Receptor Blocking Solution)	BioLegend	Cat# 422302; RRID: AB_2818986
APC Mouse Anti-Human CD206 (19.2)	BD Pharmingen	Cat# 550889; RRID: AB_398476
SOX2 (D6D9) XP Rabbit mAb	Cell Signaling Technology	Cat# 3579, RRID: AB_2195767
Human/Mouse TSG-6 Antibody	R&D systems	Cat# MAB2104, RRID: AB_2204654
Anti-TSG6 antibody [EPR17582-45]	Abcam	Cat# ab267469, RRID: AB_3675282
OLIG2 antibody	Proteintech	Cat# 13999-1-AP, RRID: AB_2157541
Anti-EGF antibody [EPR19899]	Abcam	Cat# ab206423, RRID: AB_3675283
Anti-EGF antibody	ThermoFisher Scientific	Cat# MA5-42471, RRID: AB_2911612
EGF Receptor (D38B1) XP® Rabbit mAb	Cell Signaling Technology	Cat# 4267BF, RRID: AB_2895042
Phospho-EGF Receptor (Tyr1068) (D7A5) XP® Rabbit mAb	Cell Signaling Technology	Cat# 3777, RRID: AB_2096270
Stat6 (D3H4) Rabbit mAb	Cell Signaling Technology	Cat# 5397, RRID: AB_11220421
Phospho-Stat6 (Tyr641) Antibody	Cell Signaling Technology	Cat# 9361, RRID: AB_331595
Phospho-Akt (Ser473) (D9E) XP® Rabbit mAb	Cell Signaling Technology	Cat# 4060, RRID: AB_2315049
Akt (pan) (C67E7) Rabbit mAb	Cell Signaling Technology	Cat# 4691, RRID: AB_915783
Phospho-mTOR (Ser2448) (D9C2) XP Rabbit mAb	Cell Signaling Technology	Cat# 5536, RRID: AB_10691552
mTOR (7C10) Rabbit mAb	Cell Signaling Technology	Cat# 2983, RRID: AB_2105622
Mouse Anti-beta Tubulin	Abcepta	Cat# AM1031a, RRID: AB_1968384
TLR4 Monoclonal antibody	Proteintech	Cat# 66350-1-Ig, RRID: AB_2881730
MYD88 Monoclonal antibody	Proteintech	Cat# 67969-1-Ig, RRID: AB_2918720
Anti-Human CD107a / LAMP1 (H4A3)	Proteintech	Cat# 65051-1-Ig, RRID: AB_2881467
Phospho-NF-κB p65 (Ser536) (93H1) Rabbit mAb	Cell Signaling Technology	Cat# 3033, RRID: AB_331284
NF-kappaB p65 (D14E12) XP Rabbit mAb	Cell Signaling Technology	Cat# 8242, RRID: AB_10859369
Biological samples		
Fresh GBM samples (used for isolation of primary TAMs)	The First Affiliated Hospital of Nanjing Medical University	N/A
Frozen GBM samples	The First Affiliated Hospital of Nanjing Medical University	N/A
Paraffin GBM samples	The First Affiliated Hospital of Nanjing Medical University	N/A
Peripheral blood samples of healthy donors (used for isolation of PBMC)	This paper	N/A
Chemicals, peptides, and recombinant proteins		
Deoxyribonuclease I from bovine pancreas	Sigma-Aldrich	Cat# DN25
Dispase® II (neutral protease, grade II)	Roche	Cat# 04942078001
Collagenase Type IV	Gibco	Cat# 17104019
EasySep™ Buffer	Stem Cell Technologies	Cat# 20144
Lymphoprep™	Stem Cell Technologies	Cat# 07801
BD Pharm Lyse™ Lysing Buffer	BD Biosciences	Cat# 555899; RRID: AB_2869057
Bovine Serum Albumin (BSA)	Yeasen Biotechnology	Cat# 36101ES60
RPMI 1640 Medium	Gibco	Cat# C11875500CP
DMEM/High glucose with L-glutamine	Cytiva	Cat# SH30022.01
Neurobasal™-A Medium	Gibco	Cat# 10888022
Neurobasal™ Medium	Gibco	Cat# 21103049
Sodium Pyruvate (100 mM)	Gibco	Cat# 1136070

(Continued on next page)

Continued

REAGENT or RESOURCE	SOURCE	IDENTIFIER
GlutaMAX™ Supplement	Gibco	Cat# 35050061
Recombinant Human EGF Protein	R&D Systems	Cat# 236-EG
Recombinant Human FGF basic	R&D Systems	Cat# 4114-TC
B-27™ Supplement (50X), minus vitamin A	Gibco	Cat# 12587010
Penicillin-Streptomycin (10,000 U/mL)	Gibco	Cat# 15140122
Fetal Bovine Serum	Sigma-Aldrich	Cat# F8318
CellTiter-Glo Luminescent Cell Viability Assay	Promega	Cat# G7571
D-Luciferin	Yeasen Biotechnology	Cat# 40902ES08
Dimethyl Sulfoxide	Sigma-Aldrich	Cat# D2650
DAPI Staining Solution	Beyotime	Cat# C1006
AS1517499	MedChemExpress	Cat# HY-100614
Osimertinib	MedChemExpress	Cat# HY-15772
Gefitinib	MedChemExpress	Cat# HY-50895
Colistin	MedChemExpress	Cat# HY-113678

Critical commercial assays

Four-color multiple fluorescent immunohistochemical staining kit	Absin	Cat# abs50012
Human TNF-α ELISA Kit	Absin	Cat# abs510006
Human Tumor necrosis factor-inducible gene 6 protein (TNFAIP6) ELISA kit	Cusbio	Cat# CSB-EL023959HU

Deposited data

GBM scRNA-seq data (Dataset A)	This paper	NGDC: HRA004899
GBM scRNA-seq data (Dataset B)	Abdelfattah et al. ²⁹	GEO: GSE182109
GBM snRNA-seq data (Dataset C)	Wang et al. ³⁰	CPTAC: phs001287
RNA-seq and ChIP-seq data of GSC and NSC	Mack et al. ³⁴	GEO: GSE119776
H3K27ac ChIP-seq data of GSC and DGC	Suvà et al. ³⁵	GEO: GSE54792

Experimental models: Cell lines

293FT	ThermoFisher Scientific	Cat# R70007
Human: ENSA	Millipore Sigma	Cat# SCC003
Human: NSC11	Alstem	Cat# hNSC11
Human: THP-1	ATCC	Cat# TIB-202
Human: Cal27	ATCC	Cat# CRL-2095
Human: AGS	ATCC	Cat# CRL-1739

Experimental models: Organisms/strains

NCG mice (NOD/ShiLtJGpt-Prkdc ^{em26Cd52} Il2rg ^{em26Cd22} /Gpt)	GemPharmatech (Nanjing, China)	Strain NO. T001475
huHSC-NCG mice (huCD34+HSC-NOD/ShiLtJGpt-Prkdc ^{em26Cd52} Il2rg ^{em26Cd22} /Gpt (CH)	GemPharmatech (Nanjing, China)	Strain NO. T037620

Oligonucleotides

qPCR Primers sets, see Table S1	This paper	N/A
---------------------------------	------------	-----

Recombinant DNA

pLKO.1 non-targeting vector	Sigma-Aldrich	Cat# SHC002
pCMV-dR8.2 dvpr	Stewart et al. ⁶⁶	Addgene Plasmid # 8455
pCI-VSVG	A gift from Garry Nolan (Stanford Cancer Institute)	Addgene Plasmid # 1733

Software and algorithms

GRCh38 (Reference-2020-A-2.0.0)	10x Genomics	https://support.10xgenomics.com/single-cell-atac/software/downloads/latest
Cellranger (v7.1.0)	10x Genomics	https://support.10xgenomics.com/single-cell-gene-expression/software/pipelines/

(Continued on next page)

Continued

REAGENT or RESOURCE	SOURCE	IDENTIFIER
Harmony (v0.1.0)	Korsunsky et al. ⁶⁷	https://github.com/immunogenomics/harmony
Seurat (v4.1.1)	Satija et al. ⁶⁸	https://satijalab.org/seurat/
GlioVis	Bowman et al. ⁴³	http://gliovis.bioinfo.cnio.es
FlowJo (v10.8.1)	BD Biosciences	https://www.flowjo.com/solutions/flowjo
GraphPad Prism (v9.3.1)	GraphPad Prism	https://www.graphpad.com
Adobe Illustrator (v27.0)	Adobe	https://www.adobe.com/products/illustrator.html
EndNote (v20.2)	Clarivate	https://endnote.com

EXPERIMENTAL MODEL AND STUDY PARTICIPANT DETAILS

Patients and human tumor samples

Paraffin-embedded (n = 30) and fresh tumor (n=20) samples were obtained from patients with GBM who received surgical resection from the Department of Neurosurgery, the First Affiliated Hospital of Nanjing Medical University. The diagnosis of GBM was confirmed independently by two experienced pathologists.

Patient-derived and cell line models

All related procedures for collecting samples from patients in the First Affiliated Hospital of Nanjing Medical University were performed with the approval of the internal review and ethics boards of the First Affiliated Hospital of Nanjing Medical University (2021-SR-076). Informed consent was provided for patients to collect samples. The research is not intended to provide direct medical or financial benefit to anyone including the donor.

GBM tissues for GSC isolation were obtained from excess surgical resection samples from patients at the Case Western Reserve University (Cleveland, OH) after review by neuropathology with appropriate consent and in accordance with an Institutional Review Board-approved protocol (090401). All patient studies were conducted in accordance with the Declaration of Helsinki. To minimize in vitro cell culture-based artifacts, patient-derived xenografts were propagated as a renewable source of GSCs. Short tandem repeat analyses were performed on the tumor model for authentication. All GSC lines were cultured in Neurobasal media (Gibco) supplemented with B27 without vitamin A (Gibco), EGF and bFGF (20 ng/mL each; R&D Systems), sodium pyruvate (catalog no. 11360070; Life Technologies), and Glutamax (catalog no. 35050061; Life Technologies) at 37°C with 20% oxygen and 5% carbon dioxide. All cells were thawed within 1 month of these experimental procedures. Further, details of these patients are restricted by the institutional requirements. All experiments conform to relevant regulatory standards.

This study used the nonmalignant NSC models ENSA and NSC11. ENSA (ENStem-A) is a human neural progenitor cell (Millipore Sigma, Cat# SCC003). NSC11 is a human-induced pluripotent-derived neural progenitor cell (Alstem, Cat# hNSC11).

293FT cells (ThermoFisher Scientific, Cat# R70007) were used to generate lentiviral particles as described in the method details section. They were cultured in DMEM medium (Hyclone) containing 10% fetal bovine serum (FBS, Gibco).

Human THP-1 cell lines and PBMC were cultured in RPMI/1640 medium supplemented with 10% FBS and 1% PS.

The HNSC cell line Cal27, derived from squamous cell carcinomas of the tongue, and the human gastric adenocarcinoma cell line AGS were cultured in DMEM medium (Hyclone) containing 10% fetal bovine serum (FBS, Gibco).

STR analyses were performed on cell lines used in this article for authentication.

Mice

The NCG mice (NOD/ShiLtJGpt-Prkdc^{em26Cd52}Il2rg^{em26Cd22}/Gpt, Strain NO. T001475, GemPharmatech, Nanjing, China) or the humanized immune system (HIS) mouse, huHSC-NCG mice (huCD34+HSC-NOD/ShiLtJGpt-Prkdc^{em26Cd52}Il2rg^{em26Cd22}/Gpt (CH), Strain NO. T037620, GemPharmatech, Nanjing, China) were purchased from GemPharmatech Co., Ltd (Nanjing, China). Healthy, wild-type male or female mice of NSG background (4–6 weeks old), and male or female huHSC-NCG mice (14–16 weeks old), with no prior treatment or procedures, were randomly selected and used in this study. Mice were maintained in 12 hours light/12 hours dark cycle at a room temperature of 20°C–26°C by animal husbandry staff at the Nanjing Medical University, with no more than five mice per cage. Animals had free access to water and food. Experimental animals were housed together. Housing conditions and animal status were supervised by a veterinarian. According to the ethical regulations, animals were monitored until neurological signs were observed, at which point they were sacrificed. Neurological signs or signs of morbidity included hunched posture, gait changes, lethargy, and weight loss. All murine experiments were performed under an animal protocol approved by the Institutional Animal Care and Use Committee (IACUC-2006033-2) at Nanjing Medical University in accordance with NIH and institutional guidelines.

METHOD DETAILS

Isolation and differentiation of PBMC

Human peripheral blood mononuclear cells (PBMC) were isolated from human blood by Ficoll-Paque PLUS (GE Healthcare). Briefly, human blood was diluted with an equal volume of PBS and thoroughly blended. The blood dilution was then placed over a half-volume of Ficoll-Paque PLUS and centrifuged at 2,000 rpm for 20 min. Cells from the middle layer were collected in 15ml tubes. After washing and erythrocyte lysis, cells were cultured in RPMI/1640. Then, suspended cells were washed away with PBS, and the adherent monocytes were trypsinized and subjected to differentiation steps. For the PBMC differentiation assay, cells were cultured in RPMI/1640 medium supplemented with 10% FBS, 1% PS, and 200 ng/ml M-CSF (PeproTech, 300-25-10). After seven days, cells were cultured with 100 ng/ml LPS and 20 ng/ml IFN γ for another 48 hours to obtain M1-like macrophages.

Differentiation of THP-1 cells

Human THP-1 cells were differentiated into the M0 stage with the stimulation of 50 ng/ml PMA (Sigma, P1585) for 24 hours. Then, M0 cells were cultured with 100 ng/ml LPS (Sigma, L6529) and 20 ng/ml IFN γ (PeproTech, GF305) for another 48 hours to obtain M1-like macrophages. The differentiated THP-1 cells were washed in fresh RPMI/1640 media (Gibco) and cultured in RPMI/1640 media for further experiments.

In vivo tumorigenesis

Intracranial xenografts were generated by implanting 2×10^4 human-derived GSCs into the right cerebral cortex of NCG mice (NOD/ShiLtJGpt-Prkdc^{em26Cd52}Il2rg^{em26Cd22}/Gpt, Strain NO. T001475, GemPharmatech, Nanjing, China) or the humanized immune system (HIS) mouse, huHSC-NCG mice (huCD34+HSC-NOD/ShiLtJGpt-Prkdc^{em26Cd52}Il2rgem26Cd22/Gpt (CH), Strain NO. T037620, GemPharmatech, Nanjing, China) at a depth of 3.5 mm. For co-implantation, 2×10^4 GSCs plus 2×10^4 pTAMs were implanted into the right cerebral cortex of NCG mice.

To deplete mouse monocyte-derived TAMs in GBM xenografts, mice were treated with Clodronate liposomes (50 mg/kg) through intraperitoneal (IP) injection 7 days before GSC transplantation.³²

To evaluate tumor volume, animals were monitored until neurological signs were observed in any one of the groups, at which point two mice of each group were selected randomly, and their brains were harvested and fixed in 4% formaldehyde, cryopreserved in 30% sucrose, and then cryosectioned. Hematoxylin and eosin (H&E) staining was performed on sections for histological analysis. In parallel survival experiments, mice were observed until the development of neurological signs. The maximal tumor burden was strictly limited to 1.2cm in diameter for mice, with a total tumor weight not exceeding 10% of the mice body weight.

Spatial transcriptomics data processing

The visualization of spatial gene expression is implemented in the SPATA software *SPATA::plotSurfaceInteractive*.²⁸ Pathway analyses are all implemented into our SPATA toolbox. The analysis was performed through the gene set variation analysis (GSVA) package.⁶⁹

Single-cell RNA analysis

Raw scRNA-seq data were preprocessed using Cell Ranger (v7.1.0, 10X Genomics), followed by quality filtering, doublet removal, data normalization, assessment, and correction of batch effects. Briefly, cells expressing fewer than 500 genes or genes with fewer than 1000 unique molecular identifiers (UMI) were removed. Likely dying or apoptotic cells with >15% of transcripts derived from the mitochondrial genome were also excluded. Additional possible doublets were further identified and removed. Seurat (v4.1.1)⁶⁸ was applied for data normalization, unsupervised cell clustering, and identification of differentially expressed genes among cell clusters. The cell types were defined based on cluster distribution, cluster-specific genes, unique expression of canonical cell markers, and transcriptional factors.⁶⁷

Signaling signature analysis

As for signaling signature, the pro-inflammatory signature was derived from MSigDB, standard name: GOBP_POSITIVE_REGULATION_OF_ACUTE_INFLAMMATORY_RESPONSE, systematic name: M11700 (https://www.gsea-msigdb.org/gsea/msigdb/human/geneset/GOBP_POSITIVE_REGULATION_OF_ACUTE_INFLAMMATORY_RESPONSE). The analyses of GSC signature were performed as reported previously.^{70,71} The signature score is calculated by Gene Set Enrichment Analysis (GSEA).^{72,73}

Lentiviral production and transfection

Lentiviral clones expressing two non-overlapping shRNAs directed against human TNFAIP6 (TRCN0000046913 and TRCN0000046914), or a nontargeting control shRNA (TRCN0000231489) that matches the unexpressed sequence in the human genome were obtained from Sigma-Aldrich. All shRNAs were assayed for knockdown efficiency by qRT-PCR and were then used for functional assays. Lentiviral overexpression plasmid for full-length human TNFAIP6 was generated by cloning the full-length open reading frames (ORF) into the pCDHMCS-T2A-Puro-MSCV vector (System Biosciences) using In-Fusion HD Cloning Kit

(Clontech Laboratories). Lentiviral particles were generated in 293FT cells in Neurobasal complete medium (Life Technologies) with co-transfection with the packaging vectors pCMV-dR8.2 dvpr⁶⁶ and pCI-VSVG (Addgene) using the standard calcium phosphate transfection method.

Cell proliferation assay

Cell proliferation experiments were conducted by plating cells of interest at a density of 1000 cells/well in a 96-well plate with six replicates. CellTiter-Glo (Promega, Madison, WI, USA) was used to measure cell proliferation. All data were normalized to day 1 and presented as mean \pm SEM. For the co-culture system, we stimulated GSCs with the supernatant of pTAMs derived from PBMC-induced M1-like phenotype macrophages.

Neurosphere formation assay

Decreasing numbers of cells per well (50, 20, 10, 5, and 1) were plated into 96-well plates. The presence and number of neurospheres in each well were recorded five days after plating. Extreme limiting dilution analysis was performed using software available at <http://bioinf.wehi.edu.au/software/elda>, as previously described.^{74,75} All tumorsphere and proliferation experiments were performed at least six times.

Quantitative RT-PCR

Trizol reagent (Sigma Aldrich) was used to isolate total cellular RNA from cell pellets. The qScript cDNA Synthesis Kit (Quanta Biosciences) was used for reverse transcription into cDNA. Quantitative real-time PCR was performed using Applied Biosystems 7900HT cycler using SYBR-Green PCR Master Mix (Thermo Fisher Scientific). The sequences of primers for qRT-PCR analysis were included in Table S1.

Western blotting

Cells or GBM tissues were lysed in moderate RIPA lysis buffer (50 mM Tris-HCl pH 7.4, 150 mM NaCl, two mM EDTA, 1% NP-40, 0.1% SDS, and supplemented with protease inhibitors) for 30 min at 4 °C. Cell lysates were then centrifuged at 13,000 \times g for 15 min at 4 °C. The supernatant was collected and boiled with SDS sample buffer at 100 °C for 5 min. Protein lysates were then separated through SDS-PAGE and transferred onto PVDF membranes. The membranes were blocked with 5% non-fat milk for two hrs at room temperature and then immunoblotted with indicated primary and secondary antibodies.

Co-immunoprecipitation

For the Immunoprecipitation assay, cells were lysed in NP40 lysis buffer (beyotime, P0013F) supplemented with protease and phosphatase inhibitor for 1 hour at 4 °C. Centrifuging at 13,000 \times g for 15 min at 4 °C. Cell lysates were collected and incubated with IgG or indicated primary antibody in at 4 °C overnight followed by incubation with protein A/G agarose beads for 3 hours. The beads were centrifuged at 3000 \times g, washed with lysis buffer five times for 5 min each, and then boiled with SDS sample buffer at 100 °C for 5 min. The resulting protein supernatant fraction was subjected to western blot analysis as described. This study used the following antibodies for immunoprecipitation: anti-TNFAIP6 (Abcam, ab267469), anti-EGF (ThermoFisher Scientific, MA542471), and Rabbit-IgG (beyotime, A7016). Protein A+G Agarose (beyotime, P2055).

Flow Cytometry Analysis

Cells were harvested and stained with APC Mouse Anti-Human CD206 (19.2)(BD Pharmingen, 550889) at a dilution ratio of 1:50. For intracellular staining, cells were fixed in the Fixation and Permeabilization Kit (eBioscience, 00-5521-00). After being washed with Fixation and Permeabilization Buffer, the cells were stained intracellularly for 30 minutes in the dark. All samples were acquired on a BD flow cytometer and were analyzed using FlowJo (FlowJo LLC).

Immunofluorescence

GBM patient tissues or mice xenograft tissues were fixed in cold acetone for 10 min. The tissue sections were blocked with 5% BSA plus 0.3% Triton-X in PBS at room temperature and then incubated with primary antibody at 4 °C overnight. Then, the fluorescent secondary antibody was dripped on the surface for 2 hours. Nuclei were counterstained with Hoechst for 10 min. Images were captured with a Zeiss LSM700 microscope (Carl Zeiss, USA). The following primary antibodies were used for immunofluorescent staining in this study: anti-TNFAIP6 (Santa Cruz, sc-377277), anti-SOX2 (RD system, AF2018), anti-Iba1 (Abcam, ab178846), anti-CD163 (Abcam, ab182422).

Immunohistochemistry

All slides were first deparaffinized in xylene and rehydrated, followed by washing for 3 times using PBS. Slides were then incubated in goat serum dilution buffer (GSDB) for 1 hour in a wet chamber at room temperature. The slides were incubated with primary antibody diluted in GSDB overnight at 4 °C in a wet chamber. After washing three times for 10 min each with wash buffer (450 mM NaCl, 20 mM phosphate buffer, and 0.3% Triton X-100), slides were incubated with secondary antibody in GSDB for 60 min at room temperature in a wet and light-protected chamber. Slides were subsequently washed three times with the above wash buffer. Diaminobenzidine was used to stain the slides, followed by counterstaining using hematoxylin to visualize nuclei.

Molecular docking

The 3D structures of TNFAIP6 and EGF were downloaded from the RCSB Protein Data Bank. Protein-protein docking was performed using the ClusPro server, using a global rigid search to predict the binding affinity of TNFAIP6 and EGF. MOE was used to analyze the docked structures and interface residues. PyMOL was used to generate molecular graphics.

Surface plasmon resonance (SPR)

A direct binding assay format was performed to detect direct binding using a BIAcore S200 instrument (GE Healthcare). Prior to activation, the surface of the research-grade CM5 chip was pre-conditioned with two 50 μ l injections of 10 mM HCl, 50 mM NaOH, 0.1% SDS, and 0.085% H_3PO_4 at a flow rate of 100 μ l/min. TNFAIP6 was immobilized on the sensor surface using standard amine coupling, which was achieved by activating the sensor surface using 7 min injection with a mixture of 11.5 mg/ml N-hydroxysuccinimide and 75 mg/ml 1-ethyl-3-(3-dimethylaminopropyl) carbodiimide hydrochloride. Protein immobilization was performed using a 10 min injection of TNFAIP6 (10 mg/ml) in 10 mM NaAc, pH 5.0 buffer. The remaining active esters were blocked using a 7 min injection of 1M ethanolamine, pH 8.5, at a flow rate of 10 μ l/min. Reference flow cells were prepared without the protein. Denaturation was achieved with a 30 sec injection of 10 mM HCl at a flow rate of 30 μ l/min. All binding measurements were performed in PBSP, pH 7.4, at a flow rate of 30 μ l/min. Proteins were injected over the active protein and reference surface with at least 30 seconds of association and dissociation time. Surface regeneration was achieved using dissociation for a time period, allowing the response to return to baseline. SPR equilibrium binding data, consisting of Req values from 5 point concentration series, were analyzed by fitting a steady model to yield R_{max} and K_d values using BIAcore S200 evaluation software.

Bio-Layer Interferometry (BLI)

Ni-NTA biosensors were loaded with His-tag human recombinant TNFAIP6 protein (CUSABIO TECHNOLOGY LLC, Cat# CSB-EP023959HU) and then incubated with recombinant human EGF protein (R&D Systems, Cat# 236-EG) or colistin (MedChemExpress, Cat# HY-A0089) to generate an association curve (ForteBio Octet). The 60s association phase was followed by a 90s dissociation step to obtain the K_d value by the fitting curve.

In vivo drug treatment

For drug treatment, mice were treated with control DMSO vehicle, AS1517499 (20 mg/kg intraperitoneally), osimertinib (50 mg/kg, oral administration), or colistin (2 μ g/dose, intracranially).

In vivo bioluminescence analysis

To monitor tumor growth in living animals, all GSCs used for animal studies were transduced with firefly luciferase through lentiviral infection at an MOI of 0.8. GSCs expressing firefly luciferase were then intracranially implanted into athymic immunocompromised mice. To examine the tumor growth, mouse brains implanted with GSCs were monitored by bioluminescent imaging. Blinding was used to measure tumor growth when using bioluminescence analysis. Animals were treated with 120mg/ kg body weight d-luciferin intraperitoneally and anesthetized with isoflurane for the imaging analysis. The tumor luciferase images were captured using an IVIS imaging system (Spectrum CT; PerkinElmer). All animal procedures were performed in accordance with a Nanjing Medical University Institutional Animal Care and Use Committee-approved protocol. According to the ethical regulations, animals were monitored until neurological signs were observed, at which point they were sacrificed. Neurological signs or signs of morbidity included hunched posture, gait changes, lethargy, and weight loss. The maximal tumor burden was strictly limited to 1.2cm in diameter for mice, with a total tumor weight not exceeding 10% of the mice body weight.

QUANTIFICATION AND STATISTICAL ANALYSIS

Power calculations based upon previous *in vivo* studies in our models were utilized to predetermine sample sizes. The studies were designed with 80% power to detect a difference of 20% given a 10% standard deviation at a significance level of $\alpha = 0.05$. Kaplan-Meier survival curves were generated using Prism software, and a log-rank test was performed to assess statistical significance between groups. For other studies, a two-sided unpaired Student's t-test was used to assess differences between groups. Data distribution was assessed for normality using the Shapiro-Wilk test. Precise experimental details (number of animals or cells, experimental replication, definition of center, and dispersion and precision measures) are provided in the figure legends and the [experimental model and study participant details](#) and [method details](#) sections above. P values are detailed in the figure legends. P values < 0.05 were considered to be significant. No data were excluded from the analyses.